

MICROMECHANICAL MODELING OF CARBON NANOTUBE – POLYMER
COMPOSITES

A THESIS SUBMITTED TO
THE GRADUATE SCHOOL OF NATURAL AND APPLIED SCIENCES
OF
MIDDLE EAST TECHNICAL UNIVERSITY

BY

VAHİDULLAH TAÇ

IN PARTIAL FULFILLMENT OF THE REQUIREMENTS
FOR
THE DEGREE OF MASTER OF SCIENCE
IN
AEROSPACE ENGINEERING

DECEMBER 2018

Approval of the thesis:

**MICROMECHANICAL MODELING OF CARBON NANOTUBE –
POLYMER COMPOSITES**

submitted by **VAHİDULLAH TAÇ** in partial fulfillment of the requirements for the degree of **Master of Science in Aerospace Engineering Department, Middle East Technical University** by,

Prof. Dr. Halil Kalıpçılar
Dean, Graduate School of **Natural and Applied Sciences** _____

Prof. Dr. İsmail Hakkı Tuncer
Head of Department, **Aerospace Engineering** _____

Assoc. Prof. Dr. Ercan Gürses
Supervisor, **Aerospace Engineering** _____

Examining Committee Members:

Prof. Dr. Altan Kayran
Dept. of Aerospace Engineering, METU _____

Assoc. Prof. Dr. Ercan Gürses
Dept. of Aerospace Engineering, METU _____

Assoc. Prof. Dr. Demirkan Çöker
Dept. of Aerospace Engineering, METU _____

Assist. Prof. Dr. Ali Javili
Mechanical Engineering Dept., Bilkent University _____

Assist. Prof. Dr. Tuncay Yalçınkaya
Dept. of Aerospace Engineering, METU _____

Date: _____ 14/12/2018 _____

I hereby declare that all information in this document has been obtained and presented in accordance with academic rules and ethical conduct. I also declare that, as required by these rules and conduct, I have fully cited and referenced all material and results that are not original to this work.

Name, Last name: Vahidullah Taç

Signature:

ABSTRACT

MICROMECHANICAL MODELING OF CARBON NANOTUBE – POLYMER COMPOSITES

Taç, Vahidullah

MSc, Department of Aerospace Engineering

Supervisor : Assoc. Prof. Dr. Ercan Gürses

December 2018, 69 pages

A micromechanics-based model is developed to simulate carbon nanotube – polymer nanocomposites and analyze its mechanical behavior. The nanocomposite is first divided into four distinct regions, or phases, based on mechanical behavior and density; the carbon nanotube, the interface, the interphase and the polymer. The finite element method was later used to combine the nanotube and interface phases into an effective fiber for better representation and incorporation of their roles and constitutive properties in the micromechanical model. The elastic moduli of the interphase were modelled in a position dependent manner to better represent its true nature. Parametric studies were performed on the model and the results were compared with the previous work in the literature. The four phases were each found to have significant effects on the behavior of the nanocomposite. It was observed that when a soft interface model is used, the direct effect of the carbon nanotube on the stiffness of the nanocomposite vanishes, and the interphase becomes the sole reinforcement phase in the composite. Whereas in the case of a stiff interface the CNT significantly affects the mechanical

properties of the composite through the effective fiber. Thinner but longer carbon nanotubes were found to better enhance the stiffness of the nanocomposite compared to thick and short nanotubes.

Keywords: Carbon Nanotube, Micromechanics, Interface, Interphase, Nanocomposite, Homogenization

ÖZ

KARBON NANOTÜP – POLİMER KOMPOZİTLERİNİN MİKROMEKANİKSEL MODELLEMESİ

Taç, Vahidullah

Yüksek Lisans, Havacılık ve Uzay Mühendisliği

Tez Yöneticisi : Doç. Dr. Ercan Gürses

Aralık 2018, 69 sayfa

Karbon nanotüplerle güçlendirilmiş olan polimer bazlı nano kompozit malzemelerin simülasyon ve mekanik analizi için bir adet mikromekanik model geliştirilmiştir. Öncelikle adı geçen nano kompozit mekanik özellikleri ve yoğunluğuna göre karbon nanotüp, arayüz, ara-faz ve polimerden oluşan 4 farklı bölgeye veya faza ayrılmıştır. Daha sonra karbon nanotüp ve arayüz fazlarının mekanik özelliklerinin ve rollerinin mikromekanik modelde daha iyi yansıtılabilmesi için bu fazlar sonlu elemanlar modellemesiyle etkin fiber denen tek bir faza dönüştürülmüştür. Ara-faz bölgesinin daha iyi incelenebilmesi için bu fazın mekanik özelliklerinin fonksiyonel olarak biçimlendirilmesine karar verilmiştir. Modelin farklı değişkenleri üzerinde parametrik çalışmalar yapıp literatürde mevcut olan diğer çalışmalarla kıyaslamalar yapılmıştır. 4 fazın her birinin nanokompozit mekanik özelliklerini ciddi bir şekilde etkilediği görülmüştür. Arayüz fazı için yumuşak arayüz modeli kullanıldığında arayüzün yükleri karbon nanotüpe aktaramadığı için karbon nanotüpün kompozit mekanik

özelliklerini direk olarak etkilemediği görülmüştür. Bu durumda ara-faz bölgesi kompozitteki tek güçlendirme fazı haline gelmektedir. Sert arayüz modeli kullanıldığında ise karbon nanotüp kompozit özelliklerini ciddi bir şekilde etkilediği görülmüştür. Ayrıca ince ve uzun nanotüplerin kompoziti kalın ve kısa nanotüplerden daha çok güçlendirdiği görülmüştür.

Anahtar Kelimeler: Karbon Nanotüp, Mikromekanik, Arayüz, Ara-faz, Nanokompozit, Homojenleştirme

I dedicate my thesis to my parents, who through thick and thin, have been there for me. Their support and drive are what have made me who I am.

ACKNOWLEDGMENTS

The author wishes to express his deepest gratitude to his supervisor Assoc. Prof. Dr. Ercan Gürses for his unrelenting guidance, advice, criticism, encouragements and insight throughout this research work.

TABLE OF CONTENTS

ABSTRACT	v
ÖZ	vii
ACKNOWLEDGMENTS	x
TABLE OF CONTENTS.....	xi
LIST OF TABLES.....	xiii
LIST OF FIGURES	xiv
LIST OF SYMBOLS AND ABBREVIATIONS.....	xvii
CHAPTERS	
1. INTRODUCTION.....	1
1.1 Carbon Nanotubes	1
1.2 Carbon Nanotube – Polymer Composites.....	5
1.3 Micromechanics	6
1.3.1 J.D. Eshelby.....	6
1.3.2 Mori-Tanaka	9
1.3.3 Qu.....	10
2. MICROMECHANICAL MODEL	13
2.1 Literature Review	13
2.2 Definition of the Model	16
2.3 Orientation Averaging.....	19
2.4 Moduli of the Micromechanical Phases.....	20
2.4.1 Carbon Nanotubes (CNT)	20
2.4.2 Interface (IF).....	21

2.4.3 Effective Fiber (EF)	22
2.4.3.1 Young's Modulus E_1 in the Longitudinal Direction.....	26
2.4.3.2 Young's Modulus E_2 in the Transverse Direction and Poisson's ratio ν_{12}	27
2.4.3.3 Shear Modulus G_{12} and Poisson's ratio ν_{23}	28
2.4.3.4 Verification with a Rheological Model.....	30
2.4.4 Interphase (IP)	33
2.4.5 Bulk Polymer (BP).....	38
3. RESULTS AND DISCUSSION.....	39
3.1 Results	39
3.1.1 Number of Inclusions	39
3.1.2 Interphase Modulus Distribution	41
3.1.3 Contributions of the Phases	43
3.1.4 Interphase Thickness	46
3.1.5 CNT Orientation Distribution.....	47
3.1.6 CNT Aspect Ratio	48
4. CONCLUSIONS	51
4.1 Recommendations and Future Work	52
REFERENCES.....	53
APPENDICES	
APPENDIX A	57
APPENDIX B	59
APPENDIX C	65

LIST OF TABLES

TABLES

Table 1. Elastic coefficients of carbon nanotubes as a function of the CNT radius (source: [24]).	21
Table 2: Transverse elastic constants of the effective fiber with a stiff interface model ($EIF = 5 E_{polymer}$)	30
Table 3: Transverse elastic constants of the effective fiber with a soft interface model ($EIF = 0.3 E_{polymer}$)	30
Table 4: Longitudinal Young's modulus of the effective fiber for the three CNT radii and the stiff interface model calculated with the rheological model.	32
Table 5: Longitudinal Young's modulus of the effective fiber for the three CNT radii and the soft interface model calculated with the rheological model.	33

LIST OF FIGURES

FIGURES

Figure 1. An illustration of a carbon nanotube.....	2
Figure 2. Carbon nanotube chirality vector.....	2
Figure 3. 5 walled (a), double walled (b) and 7 walled (c) carbon nanotubes as observed by Iijima [1].	3
Figure 4. Young’s modulus of various high-performance engineering materials as compared to carbon nanotubes.	4
Figure 5. Ultimate strength of various high-performance engineering materials as compared to carbon nanotubes.	4
Figure 6. Graphical representation of the phases in the micromechanical model used in this study.....	16
Figure 7. Sequence of operations in the current micromechanical model.	17
Figure 8. Mori-Tanaka distribution of micromechanical inclusions (a), and the distribution in an actual carbon nanotube composite (b).....	23
Figure 9: Isometric views of finite element models consisting of CNT and the interface (left), and effective fiber (right).....	24
Figure 10. Side views of finite element models consisting of CNT and the interface (left), and effective fiber (right).	25
Figure 11: Sequence of operations in the current model.....	26
Figure 12: Loading conditions used to obtain the longitudinal modulus of the effective fiber.	27
Figure 13: Loading conditions used to obtain the transverse modulus and Poisson’s ratio ν_{12} of the effective fiber.....	28
Figure 14: Loading conditions used to obtain G_{12}	29
Figure 15. Partitioning of the CNT and interface model into four regions.	31
Figure 16. Simplification of the 4 regions in the CNT + interface model with linear springs.	32
Figure 17. Density distribution of a PI-CNT composite in the radial direction originating in the center of the CNT. Image courtesy of [24].....	34
Figure 18. Atomistic images of the interphase region in a Poly Vinyl Chloride (PVC) – CNT Composite (top) and density distribution of Poly Vinyl Chloride (PVC) in the radial direction from surface of the CNT (bottom). Image obtained from [37].....	35

Figure 19: Representative Young's modulus distribution across the micromechanical model.	37
Figure 20. Illustrated AFM measurement of the local shear modulus around a TiO ₂ - Elastomer nanocomposite. Note that the abscissa of the plot on the right side corresponds to the white line crossing the nanoparticle on the left side. Image obtained from [39]......	37
Figure 21. Representative Young's modulus of CNT-Natural Rubber nanocomposite and its corresponding modulus-length curve to represent the interphase thickness. Image obtained from [40]......	38
Figure 22. Comparison of 2-phase, 3-phase and 4-phase micromechanical models.	40
Figure 23. Normalized composite moduli vs CNT radius for various interphase moduli distributions.	42
Figure 24. Contribution of each phase to the modulus of the nanocomposite when using a stiff interface model.....	45
Figure 25. Contribution of each phase to the modulus of the nanocomposite when using a soft interface model.	46
Figure 26. Results of the current model using a CNT radius of 3.9 Å, interphase thickness of 3 Å, and $a = 5$ compared to experimental and numerical findings in the literature [14,41,42]......	47
Figure 27: Composite moduli vs effective fiber vol.% for aligned and random inclusion distributions.	48
Figure 28: Composite Young's and shear moduli vs effective fiber aspect ratio	49
Figure 29. Number of iterations needed to converge given a maximum tolerance in infinite medium Young's and shear moduli.....	58
Figure 30. Cylindrical (left), spherical (center) and plate-like (right) inclusion shapes.	60
Figure 31. Variation of normalized composite Young's modulus, E/E_{BP} as a function of inclusion volume fraction for cylindrical, spherical and plate-like inclusions.	61
Figure 32. Variation of normalized composite Young's modulus as a function of cylindrical inclusion aspect ratio (left) and plate-like inclusion aspect ratio (right).	62
Figure 33. Variation of normalized composite stiffness with respect to cylindrical inclusion radius (top left), spherical inclusion radius (top right), and plate-like inclusion radius (bottom).	62
Figure 34. Variation of axial displacement in axial loading as a function of effective fiber moduli.....	66
Figure 35. Variation of radial displacement in radial loading as a function of effective fiber moduli.....	67

Figure 36. Variation of axial displacement in radial loading as a function of effective fiber moduli.....	68
Figure 37. Variation of hoop displacement in torsional loading as a function of effective fiber moduli.....	69

LIST OF SYMBOLS AND ABBREVIATIONS

SYMBOLS AND ABBREVIATIONS

Symbol/Abbreviation	Description
CNT	Carbon Nanotube
MWCNT	Multi-Walled Carbon Nanotube
DWCNT	Double-Walled Carbon Nanotube
SWCNT	Single Walled Carbon Nanotube
\mathbf{C}	Composite elasticity moduli tensor
\mathbf{C}_m	Matrix elasticity moduli tensor
\mathbf{C}_p	Inclusion elasticity moduli tensor
\mathbf{I}	Fourth order identity tensor
\mathbf{S}	Eshelby's tensor
v	Volume fraction
v_p	Inclusion volume fraction
δ_{ij}	Kronecker delta
\mathbf{A}	Strain concentration tensor
f_m	Matrix volume fraction
f_p	Inclusion volume fraction
σ	Stress tensor
n	Surface normal
u	Displacement vector
α	Compliance of interface in tangential direction
β	Compliance of interface in normal direction
ϵ	Strain tensor
IF	Interface
IP	Interphase
BP	Bulk Polymer
\mathbf{C}^{inf}	Elasticity moduli tensor of the infinite medium
f	Volume fraction
$\delta(x - x_0)$	Dirac's delta function
$E_{polymer}$	Polymer Young's modulus
EF	Effective Fiber
FEA	Finite Element Analysis
FEM	Finite Element Modeling
E_{IF}	Interface Young's modulus
PI	Polyamide
E_{EF}	Effective Fiber Young's Modulus
AFM	Atomic Force Microscopy
a	Interphase Young's modulus exponential decay rate
E_{BP}	Bulk polymer Young's modulus

G_{BP}

Bulk polymer shear modulus

CHAPTER 1

INTRODUCTION

This thesis is a summary of the research work that the author has performed during his studies at the department of Aerospace Engineering at Middle East Technical University on micromechanical modeling of carbon nanotube composites. This chapter is dedicated to providing introductory information about the contents, material, methods and tools used throughout the research work.

Specifically, carbon nanotubes, carbon nanotube – polymer nanocomposites and micromechanics will be explained in detail in the following subsections.

1.1 Carbon Nanotubes

Carbon nanotubes are nano-scale helical tubes entirely made out of carbon atoms. In a carbon nanotube each carbon atom forms a covalent bond, the strongest chemical bonds two atoms can make, with three other carbon atoms. The discovery of carbon nanotubes is usually attributed to Iijima [1], although they had been observed as far back as 1959 [2]. The ends of the nanotubes are usually covered with semi-spherical all-carbon structures called fullerenes. An illustration of a typical carbon nanotube with fullerenes is shown in Figure 1.

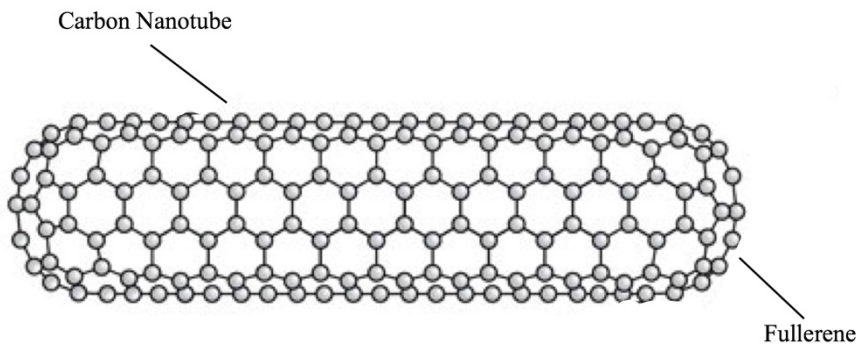


Figure 1. An illustration of a carbon nanotube.

Carbon nanotubes can be classified in a number of ways including chirality and number of layers.

In essence carbon nanotubes are rolled and seeded graphite sheets. The angle at which the hypothetical graphite sheet is rolled determines the chirality vector of the nanotube. Two important chirality vectors (n,n) and $(n,0)$ are called “armchair” and “zigzag”, respectively, as indicated in Figure 2 sourced from [3]. Any other nanotube is “chiral” with a chirality vector of (m,n) .

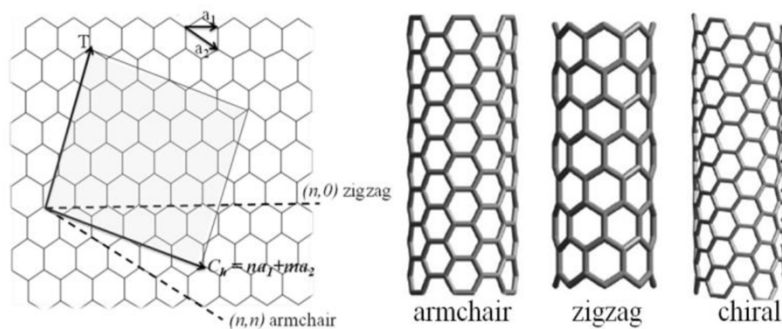


Figure 2. Carbon nanotube chirality vector.

Another way to categorize carbon nanotubes is through their number of layers. Sometimes two or more carbon nanotubes are nested in each other. In such cases the

nanotube is called a Double Walled Carbon NanoTube (DWCNT) or Multi-Walled Carbon Nanotube (MWCNT) depending on the number of layers. If there is a single layer, the nanotube is called Single Walled Carbon Nanotube (SWCNT). Double walled and multi-walled are presented in Figure 3.

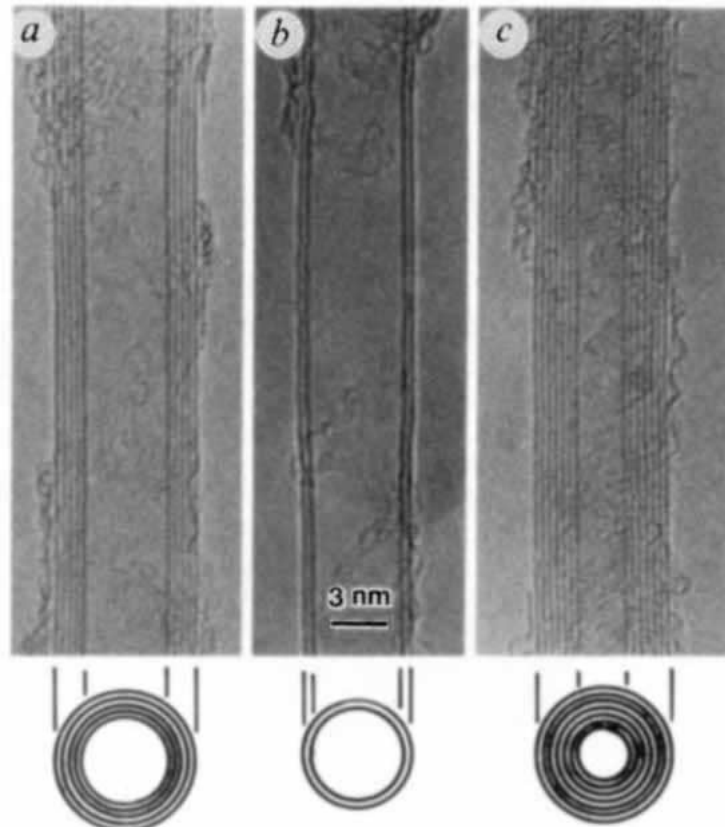


Figure 3. 5 walled (a), double walled (b) and 7 walled (c) carbon nanotubes as observed by Iijima [1].

Carbon nanotubes are often referred to as wonder materials due to their outstanding performance in multiple domains such as stiffness, strength, surface area to volume ratio, thermal and electrical conductivity and others [4]. Of particular interest to this research work is the stiffness, which is generally accepted to be above 1 TPa in the literature [5,6]. This is the highest stiffness directly observed by man to date. The stiffness and strength properties of carbon nanotubes are compared to some other commonly used high performance materials in Figure 4 and Figure 5 respectively. The data in these plots was obtained from [4].

Young's Modulus [GPa]

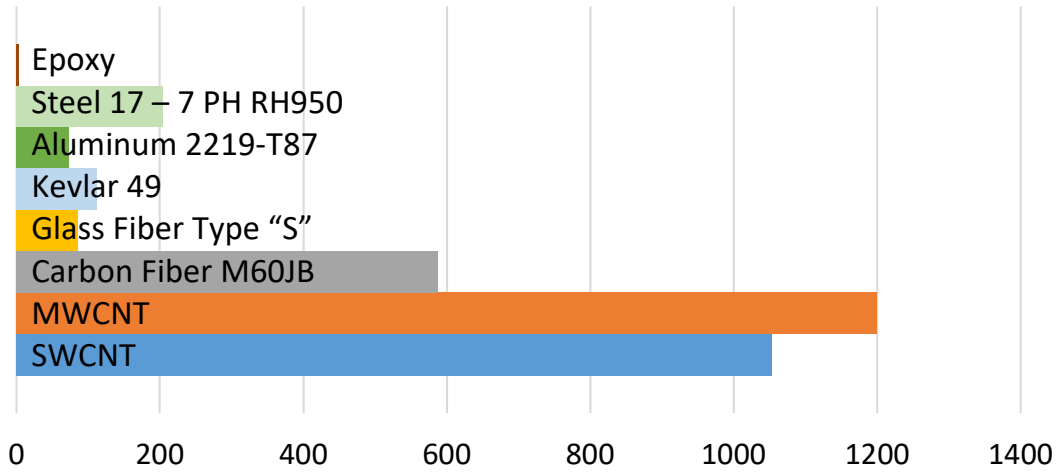


Figure 4. Young's modulus of various high-performance engineering materials as compared to carbon nanotubes.

Strength [GPa]

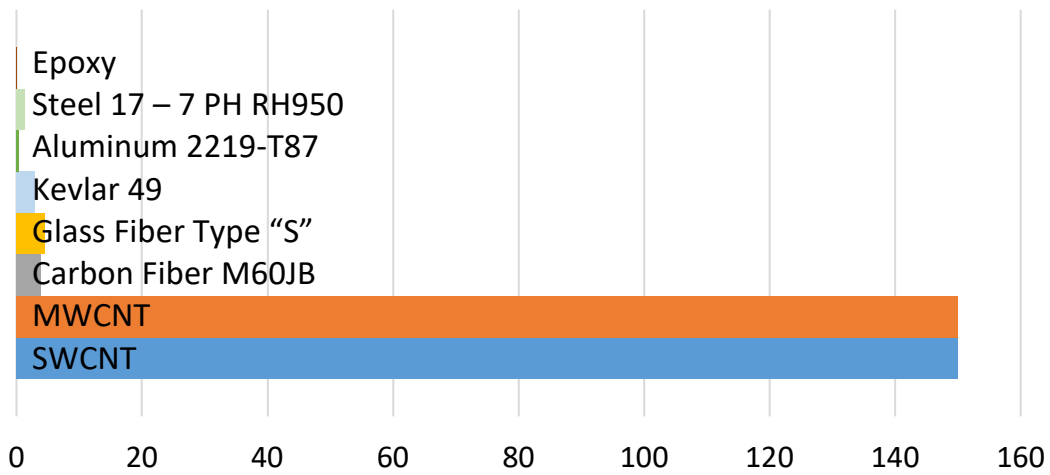


Figure 5. Ultimate strength of various high-performance engineering materials as compared to carbon nanotubes.

The aforementioned properties make carbon nanotubes some of the most highly sought-after materials in the industry, and subjects of interest in academia. They have been referred to as wonder materials due to their potential to revolutionize the materials industry in the upcoming decades. Carbon nanotubes have been suggested as the only materials that make the space elevator possible; a hypothesized structure extending to space to be used for transporting goods and humans to space [7]. While as of the date of writing of this thesis such macro-scale applications of carbon nanotubes remains distant, they are already revolutionizing the materials industry as reinforcements in polymer-based nanocomposite materials.

1.2 Carbon Nanotube – Polymer Composites

Their superior mechanical properties have helped carbon nanotubes gain much attention in the study of reinforcements for polymer matrix composites. Their high surface area to volume ratio and aspect ratio allows maximized use of their properties in polymer-based composites. Sometimes carbon atoms in the nanotubes make bonds with the polymer atoms, in a process called functionalization. This maximizes interfacial shear strength allowing for stronger adhesion between polymer and nanotube. When not functionalized, the interface between the polymer and the nanotube is dominated by Van der Waals forces. Last but not least, under ordinary conditions nanotubes are randomly scattered in the polymer, this results in a composite with isotropic constitutive behavior, as opposed to anisotropic composites produced from macroscopic fibers.

Of particular interest to this thesis is the improvement in stiffness, or elastic moduli, of the nanocomposite as a result of addition of carbon nanotubes. The rate of improvement of the stiffness of polymers by the introduction of carbon nanotubes is reported to be up to many tens of folds [8–12].

Two issues are currently seen as the major obstacles in further advancement and popularization of carbon nanotube – polymer composites [13]:

- 1- A lack of proper understanding and modelling of the interfacial region in polymer-carbon nanotube composite.

- 2- Issues with even distribution and dispersion of nanotubes in the polymer matrix.

This thesis aims to help solve the former problem by developing a micromechanical model to represent carbon nanotube-polymer composites in mechanical analyses. Micromechanics is one of the alternatives in analyzing carbon nanotube composites, the others being production and subsequent mechanical experimentation [14–16], the finite element method [9] and atomistic simulations [10,17]. Micromechanics stands out among the alternatives by being easy to use and light but very powerful.

1.3 Micromechanics

Micromechanics refers to the study of heterogeneous mechanical domains in the level of individual heterogeneities. Analytical and computational homogenization methods are valuable tools that can be used to obtain average elastic moduli and strains in heterogeneous materials in a simple and independent manner. Development of powerful micromechanical models for the simulation and study of carbon nanotube – polymer composites could lead the way for better understanding, and hence, wider usage, as well as improved performance, of this class of composites. In the following subsections, some widely used analytical homogenization models will be introduced.

1.3.1 J.D. Eshelby

Eshelby is often credited as being the founding father of micromechanics due to the strong impact that his 1957 paper has had on micromechanics [18]. Eshelby posited a single elastic ellipsoidal region inside an infinite domain with different elastic properties than that of the domain. The infinite domain was to be loaded at infinity. Eshelby sought to find the elastic state of the inclusion and the matrix. Eshelby reached two important conclusions that form the basis of all subsequent self-consistent methods, which are;

- 1- The free strain of an elastic inclusion is linearly related to the constrained strain of the same inclusion embedded in an elastic matrix by what is known as the Eshelby tensor.
- 2- The strain in the inclusion is uniform.

These two conclusions allowed for the determination of the effective elastic properties of composite materials as follows:

$$\mathbf{C} = \mathbf{C}_m + v_p(\mathbf{C}_p - \mathbf{C}_m) \left[\mathbf{I} + \mathbf{S}[\mathbf{C}_m^{-1}(\mathbf{C}_p - \mathbf{C}_m)] \right]^{-1} \quad (1)$$

where \mathbf{C} , \mathbf{C}_m and \mathbf{C}_p are the elastic moduli tensors of the composite, matrix and inclusion, respectively. v_p is the volume fraction of the composite defined as $v_p = (\text{volume of inclusion})/(\text{volume of the composite})$, \mathbf{I} is the 4th order identity tensor and \mathbf{S} is the Eshelby tensor for the ellipsoidal inclusion.

The calculation of the Eshelby tensor is done through complex elliptical integration. However, if the inclusion is of isotropic behavior the procedure is simplified. For an isotropic ellipsoidal inclusion with radii a , b and c lying on axes x , y and z respectively, where $a > b > c$ the elements of the Eshelby tensor are given as follows [19]

$$\begin{aligned} S_{1111} &= \frac{3}{8\pi(1-\nu)} a^2 I_{11} + \frac{1-2\nu}{8\pi(1-\nu)} I_1 \\ S_{1122} &= \frac{1}{8\pi(1-\nu)} b^2 I_{12} + \frac{1-2\nu}{8\pi(1-\nu)} I_1 \\ S_{1133} &= \frac{1}{8\pi(1-\nu)} c^2 I_{13} + \frac{1-2\nu}{8\pi(1-\nu)} I_1 \\ S_{1212} &= \frac{a^2 + b^2}{16\pi(1-\nu)} I_{12} + \frac{1-2\nu}{16\pi(1-\nu)} (I_1 + I_2) \\ S_{1112} &= S_{1223} = S_{1232} = 0 \end{aligned} \quad (2)$$

The rest of the elements of the Eshelby tensor can be obtained by a cyclic permutation of the dimensions $a \rightarrow b \rightarrow c$ accompanied with the corresponding index permutation $1 \rightarrow 2 \rightarrow 3$.

The terms I are given in terms of standard elliptical integrals and are given as

$$I_1 = \frac{4\pi abc}{(a^2 - b^2)(a^2 - c^2)^{\frac{1}{2}}} [F(\theta, k) - E(\theta, k)] \quad (3)$$

$$I_3 = \frac{4\pi abc}{(a^2 - b^2)(a^2 - c^2)^{\frac{1}{2}}} \left[\frac{b(a^2 - c^2)^{\frac{1}{2}}}{ac} - E(\theta, k) \right]$$

where

$$\theta = \arcsin \sqrt{\frac{a^2 - c^2}{a^2}}, k = \sqrt{\frac{a^2 - b^2}{a^2 - c^2}} \quad (4)$$

and

$$\begin{aligned} I_1 + I_2 + I_3 &= 4\pi \\ 3I_{11} + I_{12} + I_{13} &= \frac{4\pi}{a^2} \\ 3a^2 I_{11} + b^2 I_{12} + c^2 I_{13} &= 3I_1 \\ I_{12} &= \frac{I_2 - I_1}{a^2 - b^2} \end{aligned} \quad (5)$$

and the standard elliptical integrals are defined as

$$\begin{aligned} F(\theta, k) &= \int_0^\theta \frac{dw}{(1 - k^2 \sin^2 w)^{1/2}} \\ E(\theta, k) &= \int_0^\theta (1 - k^2 \sin^2 w)^{1/2} dw \end{aligned} \quad (6)$$

If the inclusion is spherical, i.e. $a = b = c$ then Eshelby's tensor has the following compact form

$$S_{ijkl} = \frac{5\nu - 1}{15(1 - \nu)} \delta_{ij} \delta_{kl} + \frac{4 - 5\nu}{15(1 - \nu)} (\delta_{ik} \delta_{jl} + \delta_{il} \delta_{jk}) \quad (7)$$

It is interesting to note that in a spherical inclusion the Eshelby's tensor does not depend on the actual radius of the inclusion.

Another interesting case is when the inclusion is an elliptic cylinder ($c \rightarrow \infty$), in which case the elements of the Eshelby tensor become:

$$\begin{aligned} S_{1111} &= \frac{1}{2(1 - \nu)} \left[\frac{b^2 + 2ab}{(a + b)^2} + (1 - 2\nu) \frac{b}{a + b} \right] \\ S_{2222} &= \frac{1}{2(1 - \nu)} \left[\frac{a^2 + 2ab}{(a + b)^2} + (1 - 2\nu) \frac{a}{a + b} \right] \end{aligned} \quad (8)$$

$$\begin{aligned}
S_{3333} &= 0 \\
S_{1122} &= \frac{1}{2(1-\nu)} \left[\frac{b^2}{(a+b)^2} + (1-2\nu) \frac{b}{a+b} \right] \\
S_{2233} &= \frac{1}{2(1-\nu)} \frac{2\nu a}{a+b} \\
S_{2211} &= \frac{1}{2(1-\nu)} \left[\frac{a^2}{(a+b)^2} + (1-2\nu) \frac{a}{a+b} \right] \\
S_{3311} &= S_{3322} = 0 \\
S_{1212} &= \frac{1}{2(1-\nu)} \left[\frac{a^2 + b^2}{2(a+b)^2} + \frac{(1-2\nu)}{2} \right] \\
S_{1133} &= \frac{1}{2(1-\nu)} \frac{2\nu b}{a+b} \\
S_{2323} &= \frac{a}{2(a+b)} \\
S_{3131} &= \frac{b}{2(a+b)}
\end{aligned}$$

1.3.2 Mori-Tanaka

Mori and Tanaka devised a method of calculating the average internal stress in a matrix-inclusion system in which the inclusion has transformation strain¹. They also show that the stress in the matrix is composed of two parts; the average stress and the locally fluctuating stress the mean of which is trivial throughout the matrix [20]. Using the Mori-Tanaka model the effective elastic moduli of the composite become [21]:

$$\mathbf{C} = (f_m \mathbf{C}_m + f_p \mathbf{C}_p \mathbf{A})(f_m \mathbf{I} + f_p \mathbf{A})^{-1} \quad (9)$$

where f_m and f_p are the volume fractions of the matrix and the inclusion, respectively, and \mathbf{C}_m and \mathbf{C}_p are the moduli tensors of each respective phase. \mathbf{I} is the 4th order unity tensor and \mathbf{A} is a dilute strain concentration tensor given as

$$\mathbf{A} = [\mathbf{I} + \mathbf{S}(\mathbf{C}_m)^{-1}(\mathbf{C}_p - \mathbf{C}_m)]^{-1} \quad (10)$$

where \mathbf{S} is Eshelby's tensor.

¹ Transformation strain, or eigenstrain is a strain field without an associated stress field. Strains resulting from thermal expansion are one subgroup of this type of strain.

The biggest difference between Eshelby's and Mori-Tanaka models is that Eshelby's model assumes there is a single inclusion embedded in an infinitely large domain. In Mori-Tanaka type models there are multiple coaxial inclusions embedded in an infinite domain. This allows for much greater flexibility resulting in widespread use of Mori-Tanaka type models in nanocomposite modeling.

1.3.3 Qu

Qu [22] developed an approximate method for the determination of the Eshelby tensor for an ellipsoidal inclusion with a slightly weakened interface. He assumed a uniform spring layer of vanishing thickness between the inclusion and the matrix across which stresses are continuous but displacements may not be

$$\begin{aligned}\Delta\sigma_{ij}n_j &= [\sigma_{ij}(\mathbf{x})|_{S^+} - \sigma_{ij}(\mathbf{x})|_{S^-}]n_j = 0 \\ \Delta u_i &= u_i(\mathbf{x})|_{S^+} - u_i(\mathbf{x})|_{S^-} = \eta_{ij}\sigma_{jk}n_k\end{aligned}\quad (11)$$

where $\sigma_{ij}(\mathbf{x})|_{S^+}$, $\sigma_{ij}(\mathbf{x})|_{S^-}$, $u_i(\mathbf{x})|_{S^+}$ and $u_i(\mathbf{x})|_{S^-}$ represent the stresses and displacements as \mathbf{x} approaches the interface, S , from the outside (S^+) and inside (S^-), respectively, and η_{ij} is the compliance tensor of the interface and n_i is the surface normal of the interface. The case of $\eta_{ij} = 0$ corresponds to a perfect interface, while $\eta_{ij} \rightarrow \infty$ corresponds to complete debonding. A slightly weakened interface then corresponds to a small η_{ij} . Qu goes on to provide a special form for η_{ij} as

$$\eta_{ij} = \alpha\delta_{ij} + (\beta - \alpha)n_in_j\quad (12)$$

where α and β are the compliance in the tangential and normal directions to the interface. In Qu's formulation the strain in the ellipsoidal inclusion, ϵ_{ij} , in terms of the uniform eigenstrain, $\check{\epsilon}_{ij}$ as

$$\begin{aligned}\epsilon_{ij}(\mathbf{x}) &= S_{ijkl}\check{\epsilon}_{kl} + L_{klmn}L_{pqst}\check{\epsilon}_{st} \int_S \eta_{kp}G_{ijmn}(\boldsymbol{\xi} - \mathbf{x})n_qn_l ds(\boldsymbol{\xi}) \\ &\quad - L_{klmn}L_{pqst} \int_S \eta_{kp}\epsilon_{st}(\boldsymbol{\epsilon})G_{ijmn}(\boldsymbol{\xi} - \mathbf{x})n_qn_l ds(\boldsymbol{\xi})\end{aligned}\quad (13)$$

An iterative formulation is then given as

$$\begin{aligned}
\epsilon_{ij}^{(n)}(\mathbf{x}) &= S_{ijkl}\check{\epsilon}_{kl} + L_{klmn}L_{pqst}\check{\epsilon}_{st} \int_S \eta_{kp}G_{ijmn}(\xi - \mathbf{x})n_qn_l ds(\xi) \\
&\quad - L_{klmn}L_{pqst} \int_S \eta_{kp}\epsilon_{st}^{(n-1)}(\xi)G_{ijmn}(\xi - \mathbf{x})n_qn_l ds(\xi) \\
&\quad n = 1, 2, 3 \dots
\end{aligned} \tag{14}$$

The leading order solution for small η_{kp} can be found as

$$\epsilon_{ij}(\mathbf{x}) \approx \epsilon_{ij}^{(1)}(\mathbf{x}) = S_{ijkl}\check{\epsilon}_{kl} + T_{ijst}(\mathbf{x})(I_{stkl} - S_{stkl})\check{\epsilon}_{kl} \tag{15}$$

where

$$T_{ijst}(\mathbf{x}) = L_{klmn}L_{stpq} \int_S \eta_{kp}G_{ijmn}(\xi - \mathbf{x})n_qn_l ds(\xi) \tag{16}$$

and

$$G_{ijmn}(\mathbf{x}) = \frac{1}{4} [\phi_{mi,nj}(\mathbf{x}) + \phi_{mj,ni}(\mathbf{x}) + \phi_{ni,mj}(\mathbf{x}) + \phi_{nj,mi}(\mathbf{x})] \tag{17}$$

and ϕ is Green's function for an infinite medium.

An alternative form of (15) can be written as

$$\epsilon_{ij}(\mathbf{x}) = S_{ijkl}^0(\mathbf{x})\check{\epsilon}_{kl} \tag{18}$$

where modified Eshelby's tensor for an ellipsoidal inclusion with a slightly weakened interface, \mathbf{S}^0 , is given as

$$S_{ijkl}^0(\mathbf{x}) = S_{ijkl} + T_{ijst}(\mathbf{x})(I_{stkl} - S_{stkl}) \tag{19}$$

CHAPTER 2

MICROMECHANICAL MODEL

After an extensive literature review process, we identified the weaknesses of the micromechanical models currently used for modeling nanocomposites and tried to address those weaknesses with a new model. Insofar as the nature of the micromechanical model is usually not affected by the nature of the inclusion or the matrix, all micromechanical models applied to nano-scale composites regardless of the inclusion type will be discussed here. This chapter is a summary of those activities.

2.1 Literature Review

A host of analytical methodologies can be used for the simulation and mechanical analysis of nanocomposites like the finite element method, micromechanics and molecular dynamics. Each of the methods has its own set of advantages as compared to the others. For example, atomistic simulations such as molecular dynamics offer great precision and flexibility at the cost of increased solution and setup time, as well as human labor. Micromechanics on the other hand offers handy tools that can readily be applied to nanocomposite analysis without a great loss in accuracy of solutions.

The simplest micromechanical model used for modeling of carbon nanotube – polymer composites consists of a simple single-inclusion Mori-Tanaka model in which the inclusion represents the nanotube. The scientific community has long recognized the need for more sophisticated models that also incorporate the interfacial region between the nanotube and the polymer. For example Yang and Cho [23] model a nanocomposite using three phases that represent the inclusion (reinforcement), the matrix and the interfacial gap between the inclusion and the matrix. The three phases are embedded in a fictitious infinite domain that represents the nanocomposite. They

obtain the mechanical properties of the inclusion and the polymer using molecular dynamics simulations but use a curve fitting methodology for the interface.

Yang et al. [10] divide a carbon nanotube – polymer nanocomposite into 3 regions comprising of the inclusion, the matrix and the interphase; which is a region of the matrix around the nanotube with modified mechanical properties. They also recognize the weak region between the nanotube and the polymer; which is usually referred to as the interface phase. They incorporate the effects of the interface into the carbon nanotube to obtain an effective fiber. They also merge the interphase and the matrix to obtain an effective matrix. They then use a multi inclusion model with the effective fiber and the effective matrix to represent the nanocomposite. They then compare the performance of their micromechanical model with molecular dynamics simulations.

Another study done by Tsai et al. [24] replaces the carbon nanotube in the composite with a solid cylinder of equivalent mechanical properties by comparing the energy in the molecular dynamics and finite element models under identical loading conditions. An effective interphase representing the non-bonded gap between the nanotube and polymer was obtained through energy comparison. A three-phase micromechanical model was used to obtain the mechanical properties of the nanocomposite.

In a comprehensive 2003 paper Odegard et al. [14] study carbon nanotube (CNT) – polymer composites using a variety of methodologies such as equivalent continuum modeling, molecular dynamics, micromechanics and experimentation. The micromechanical model they use consists of two phases representing the effective fiber and the polymer. The properties of the carbon nanotube are obtained from molecular dynamics simulations and later turned into an effective fiber using equivalent-continuum modeling. The stiffness tensors obtained through the continuum micromechanical models are homogenized using an orientation averaging integral and compared to experimental results they obtain through synthesizing and subsequent testing of carbon nanotube composites.

Wang et al. show that Mori-Tanaka type models do not compensate for the coated or nested nature of the inclusions in a series of two papers [25,26]. They then proceed to developing a modified strain concentration factor that accounts for this phenomenon.

They model a series of CNT nanotubes with soft interface for verification of the model and comparison with the literature.

It has consistently recognized that a region of the polymer in the direct vicinity of the nanotube has elevated densities [17,24,27] making it likely that the mechanical properties are also altered in the said region. Ignoring this behavior could result in erroneous, referred to as interphase in this thesis, could play a significant, and perhaps even monopolistic role [17] in the stiffening of the nanocomposite.

Another issue seen in the micromechanical models currently offered in the literature for modeling of nanocomposites is that they tend to model the nanocomposite using 2 or at most 3 phases. This is despite the overwhelming evidence that there are at least four distinct phases, in a nanocomposite consisting of the nano inclusion, the interface (IF), the interphase (IP), and the bulk polymer (BP). The interface² refers to the interfacial gap between CNT and polymer atoms that is mostly dominated by Van der Waals forces, the interphase is a part of the polymer in the vicinity of the CNT that has position dependent properties due to electrostatic interaction with the CNT atoms, while bulk polymer refers to the rest of the polymer.

The research work reported in this thesis aims to address the aforementioned deficiencies by using a micromechanical model with multiple inclusions. The model also allows for position dependent grading of phase moduli; a property that was utilized in the interphase in this research work. The results were further improved by homogenization of the CNT and IF phases using finite element analysis. The results of the micromechanical model are then homogenized using an orientation averaging algorithm to better represent actual nanocomposites.

² The interface in this context refers to one of the phases in the nanocomposite and it has a finite volume and thickness. This may be in contrast to some other scientific lexicons where the word interface refers only to the surface through which two elements interact.

2.2 Definition of the Model

We adopt a multi-inclusion micromechanical model outlined in [28] based on the Mori-Tanaka method [20,21,29]. The model posits multiple concentric ellipsoidal phases of elastic behavior. The dimensions of the ellipsoids are given as a_1, b_1, c_1 for the first phase, a_2, b_2, c_2 for the second phase and et cetera and are thought to be similar in shape, i.e. $\frac{a_1}{a_2} = \frac{b_1}{b_2} = \frac{c_1}{c_2} = \gamma$. The inclusions are assumed to be embedded in a theoretical phase called the infinite medium. A schematic representation of the micromechanical model is given in Figure 6.

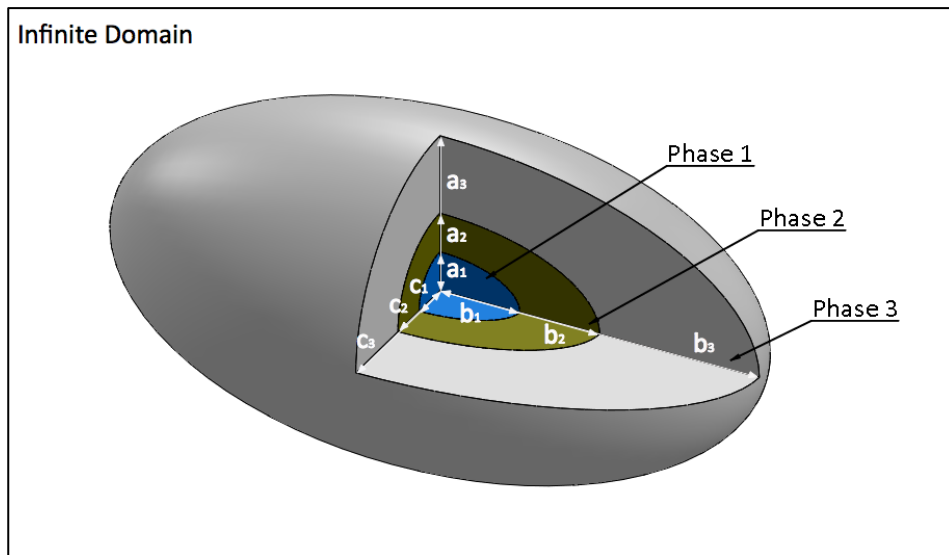


Figure 6. Graphical representation of the phases in the micromechanical model used in this study.

The infinite medium represents the final nanocomposite that is effectively homogenous, and hence a single phase in a continuum scale. To this end the calculations in the micromechanical model were iterated until the elastic moduli of the infinite medium matched the initial guesses. A flowchart that shows how the current micromechanical model works is shown in Figure 7. Further information about the determination of the elastic moduli of the infinite medium can be found in Appendix A.

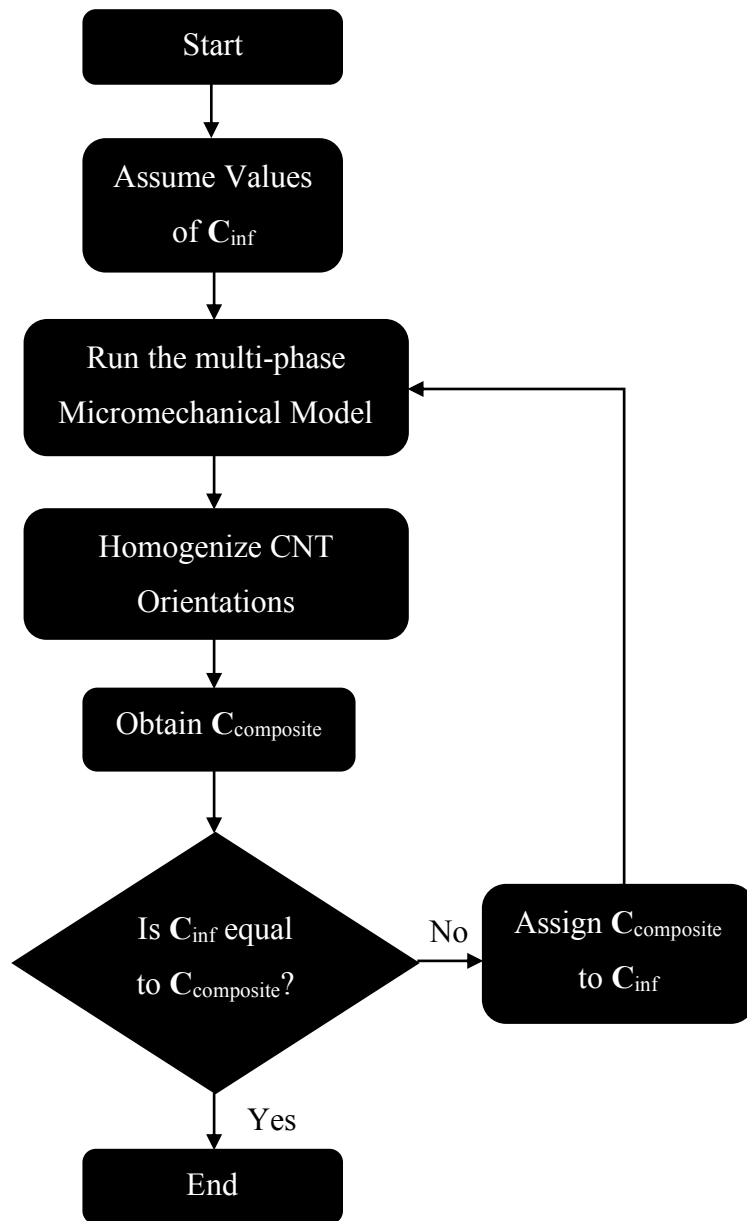


Figure 7. Sequence of operations in the current micromechanical model.

The elasticity tensor of the nanocomposite of n phases is given as

$$\begin{aligned} \mathbf{C} &= \mathbf{C}^{inf} [\mathbf{I} + (\mathbf{S} - \mathbf{I})\Lambda] [\mathbf{I} + \mathbf{S}\Lambda]^{-1} \\ \Lambda &= \sum_{i=1}^n f_i \Lambda_i \end{aligned} \quad (20)$$

where \mathbf{S} is Eshelby's tensor for an ellipsoidal inclusion, \mathbf{I} is 4th order unity tensor, f_i is the volume fraction of the i -th phase, and \mathbf{C}^{inf} is the moduli tensor of the infinite medium. Note that Eshelby's tensor depends on the aspect ratio of the inclusion. This dependency can be used to analyze inclusions of different shapes by choosing appropriate values for the inclusion aspect ratio. Although throughout this thesis only fiber-like inclusions are studied, the model can easily be adopted to study plate-like and spherical inclusions as well. This is demonstrated in Appendix B.

Parameter Λ is defined differently for phases that are graded than for those with constant moduli. For phases with constant mechanical properties Λ is given as

$$\Lambda_i = \left[(\mathbf{C}^{inf} - \mathbf{C}_i)^{-1} \mathbf{C}^{inf} - \mathbf{S} \right]^{-1} \quad (21)$$

and when the phase is functionally graded Λ is obtained by an integration scheme as follows

$$\begin{aligned} \Lambda_i &= \frac{3}{1 - \gamma^3} \int_{\gamma}^1 r^2 \lambda_i(r) dr \\ \lambda_i &= \left[(\mathbf{C}^{inf} - \mathbf{C}_i(r))^{-1} \mathbf{C}^{inf} - \mathbf{S} \right]^{-1} \\ \gamma &= \frac{a_1}{a_2} = \frac{b_1}{b_2} = \frac{c_1}{c_2} \end{aligned} \quad (22)$$

It is worth noting that among γ and f_i , two variables are dependent on the others. For example, in a 3-phase model specifying γ and f_3 also fixes the values of f_1 and f_2 as follows

$$\begin{aligned} f_1 &= (1 - f_3)\gamma^3 \\ f_2 &= (1 - f_3)(1 - \gamma^3) \end{aligned} \quad (23)$$

2.3 Orientation Averaging

Orientation averaging is used to determine the average value of a tensorial term over all orientations defined by transformation from local fiber coordinates to global coordinates. Orientation averaging is used in micromechanical modeling of non-spherical inclusions to account for the different distributions of inclusion orientation such as random and axisymmetric orientation distributions. The orientation averaging integral of a tensor \mathbf{A} is denoted as $\langle \mathbf{A} \rangle$ and is defined as [14,30]

$$\langle \mathbf{A} \rangle = \frac{\int_{-\pi}^{\pi} \int_0^{\pi} \int_0^{\pi/2} \bar{A}(\phi, \theta, \psi) g(\phi, \psi) \sin(\theta) d\phi d\theta d\psi}{\int_{-\pi}^{\pi} \int_0^{\pi} \int_0^{\pi/2} g(\phi, \psi) \sin(\theta) d\phi d\theta d\psi} \quad (24)$$

where

$$\bar{A}_{ijkl} = c_{ip}c_{jq}c_{kr}c_{ls}A_{pqrs} \quad (25)$$

c_{ij} are the direction cosines for the transformation given as

$$\begin{aligned} c_{11} &= \cos \phi \cos \psi - \sin \phi \cos \theta \sin \psi \\ c_{12} &= \sin \phi \cos \psi + \cos \phi \cos \theta \sin \psi \\ c_{13} &= \sin \psi \sin \theta \\ c_{21} &= -\cos \phi \sin \psi - \sin \phi \cos \theta \cos \psi \\ c_{22} &= -\sin \phi \sin \psi + \cos \phi \cos \theta \cos \psi \\ c_{23} &= \sin \theta \cos \psi \\ c_{31} &= \sin \phi \sin \theta \\ c_{32} &= -\cos \phi \sin \theta \\ c_{33} &= \cos \theta \end{aligned} \quad (26)$$

and g is the orientation distribution function defined as [30]

$$g(\phi, \psi) = \exp(-s_1 \phi^2) \exp(-s_2 \psi^2) \quad (27)$$

s_1 and s_2 are two parameters that control the orientation. Three significant combinations of s_1 and s_2 are given as follows

Random	$s_1 = 0$	$s_2 = 0$	$g(\phi, \psi) = 1$
Aligned	$s_1 = 0$	$s_2 = \infty$	$g(\phi, \psi) = \delta(\phi - 0)\delta(\psi - 0)$
Axisymmetric	$s_1 = k$	$s_2 = \infty$	$g(\phi, \psi) = \exp[-k\phi^2]\delta(\psi - 0)$

where $\delta(x - x_0)$ is Dirac's delta function. The three distributions, as applied to CNT-polymer composites, represent the cases in which the nanotubes are evenly and randomly oriented in all directions, all aligned in a single direction, and partially aligned in a single direction, respectively.

2.4 Moduli of the Micromechanical Phases

Before the micromechanical model can be implemented the elastic moduli of all the constituent phases must be determined. The following subsections are dedicated to explaining how the moduli of the different phases are obtained.

2.4.1 Carbon Nanotubes (CNT)

The mechanical properties of carbon nanotubes are usually characterized using a variety of methods ranging from experimental procedures [5,6,31], the finite element method [8,9,32] and atomistic modeling such as molecular dynamics [10,24]. Carbon nanotubes are usually reported to be of transversely isotropic behavior and have longitudinal Young's modulus around 1 TPa [5,6,31]. We adopt the results of Tsai et al. [24] for the moduli tensor of the carbon nanotubes. They study three sample single walled zigzag carbon nanotubes of varying radii using molecular dynamics. Then they replace carbon nanotubes with solid cylinders of the same radii as the CNTs by varying the elastic moduli of the solid cylinder in the finite element model until its elastic energy matches that of the CNT in the molecular dynamics model under various loading conditions. We adopted their results for use in our analyses and reported the moduli in Table 1.

Table 1. Elastic coefficients of carbon nanotubes as a function of the CNT radius (source: [24]).

Chirality [-]	Radius [Å]	E_1 [GPa]	G_{12} [GPa]	ν_{12} [-]	E_2 [GPa]	ν_{23} [-]
(10,0)	3.9	1382.5	1120	0.272	645	0.2
(14,0)	5.5	981.5	779.2	0.27	504	0.2
(18,0)	7.1	759.9	596.3	0.27	425	0.2

2.4.2 Interface (IF)

The interface refers to the bordering region between the CNT and the polymer. If the carbon nanotube is not functionalized, i.e. the CNT has not formed chemical bonds with the polymer atoms, the interface is a gap of approximately 3.4 Å thickness separating the CNT from the polymer [33]. The phase is dominated by Van der Waals forces that are formed between the carbon atoms of the CNT and the molecules of polymer. The interface is assumed to behave in an isotropic elastic manner. The Young's modulus of the interface was adopted from [24] while the Poisson's ratio was assumed to be equal to 0.3. This assumption was made on the basis that most isotropic materials have Poisson's ratios close to 0.3 and that this parameter does not affect the end results in a significant manner. This hypothesis was confirmed by changing the Poisson's ratio to 0.2 and 0.4 respectively and verifying that the moduli of the nanocomposite are not affected in a discernable way. Methods of calculating the elastic properties of the interface are rare, although many studies have focused on interfacial shear strength of the interface. For example Refs. [34,35] report fiber pullout studies of CNT-polymer systems which result in interface strength values depending on the fractures in the matrix. The stiffness of the interface depends on a number of factors such as the materials of the polymer and the inclusion, functionalization between the inclusion and the matrix, and a phenomenon where the polymer chains graft around the inclusion. It is expected that the interface be very soft when no chemical functionalization or polymer grafting is present in the system, while a stiffer interface is probable otherwise. To this end we study two models of the

interface corresponding to the two cases; a soft and a stiff interface. The two models assume interface stiffnesses of $0.3E_{polymer}$ and $5E_{polymer}$, respectively, where $E_{polymer}$ corresponds to the Young's modulus of the polymer, while the Poisson's ratio was kept constant and equal to that of the polymer. A similar study was previously conducted in [36]. We compare the two cases in the Figure 25, but a stiff interface was utilized in all other comparisons.

2.4.3 Effective Fiber (EF)

Mori-Tanaka based micromechanical models assume that there are multiple inclusions with different volume fractions and mechanical properties scattered evenly inside an infinite domain [25,26]. This effectively means that in such a micromechanical model the inclusions are not necessarily nested, as shown in Figure 8 (a). This is in contrast to the actual CNT-polymer composite in which the inclusions are nested as shown in Figure 8 (b). The double inclusion model proposed by Hori and Nemat-Nasser [29], used in this paper, is derived for nested inclusions but as shown in [25] this model is equivalent to the plain multiphase model of Mori-Tanaka for the case where all inclusions have the same aspect ratio. While for some cases this deficiency of the Mori-Tanaka models may not cause significant error but if the issues of stress transfer from one phase to the other are important the error caused by continued usage of the model may become too great to ignore.

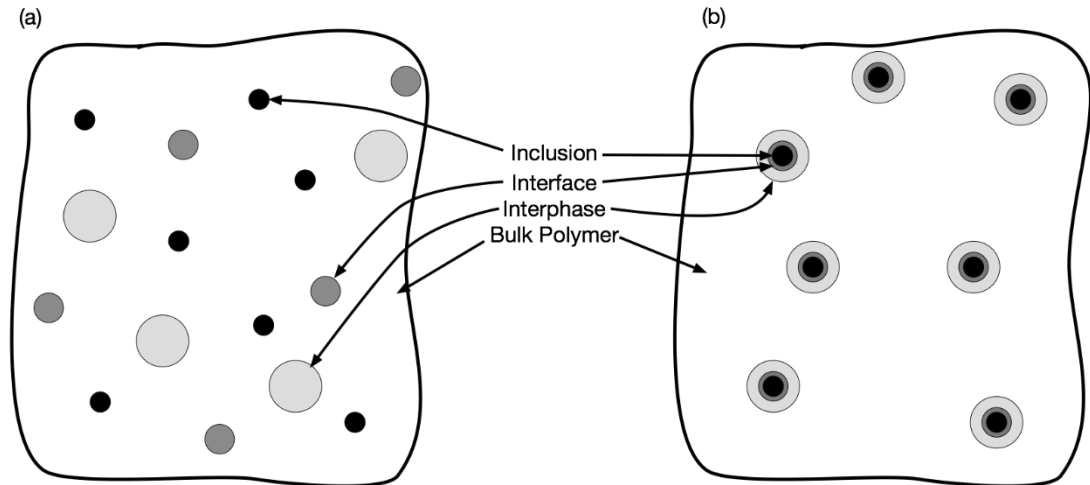


Figure 8. Mori-Tanaka distribution of micromechanical inclusions (a), and the distribution in an actual carbon nanotube composite (b).

The interface phase in the current study is a very small region with small moduli. This renders the interface insignificant if used in a purely rule-of-mixtures methodology. Rather than an insignificant small phase with trivial effect on the nanocomposite, the interface phase is seen as one of the most important phases in the nanocomposite due to its role in carrying the stresses from the polymer to the CNT. For example, if the interface is very weak the inclusion of the CNT in the micromechanical model would not make sense because it would be effectively isolated from the rest of the composite. Even if the interface is moderately stiff, it is anticipated that it will significantly alter the way the carbon nanotube performs in the nanocomposite.

To accurately model the interface resembling, as closely as possible, its true role in the physics of the nanocomposite, we decided to merge the carbon nanotube and the interface into a single phase known as the “effective fiber” using a method that accounts for the nested, or coated, nature of the CNT and interface. The finite element method stood out with its ease of use and flexibility.

To this end we prepared two sets of finite element models with three models each corresponding to the three CNT radii used in this study. In one of the sets the actual configuration of the CNT and the interface were modelled in their nested state, as shown in Figure 9 (left) and Figure 10 (left). The other set consists of a single solid

cylinder representing the effective fiber (see Figure 9 (right) and Figure 10 (right)). We applied the same loading conditions to the two sets and varied the moduli of the effective fiber model until the displacements of the two sets matched. We applied multiple loading conditions, each of which induces a different type of displacement, so as to amplify the role of a different elastic coefficient. When the displacements of the two sets matched the moduli assigned to the effective fiber were taken to be final.

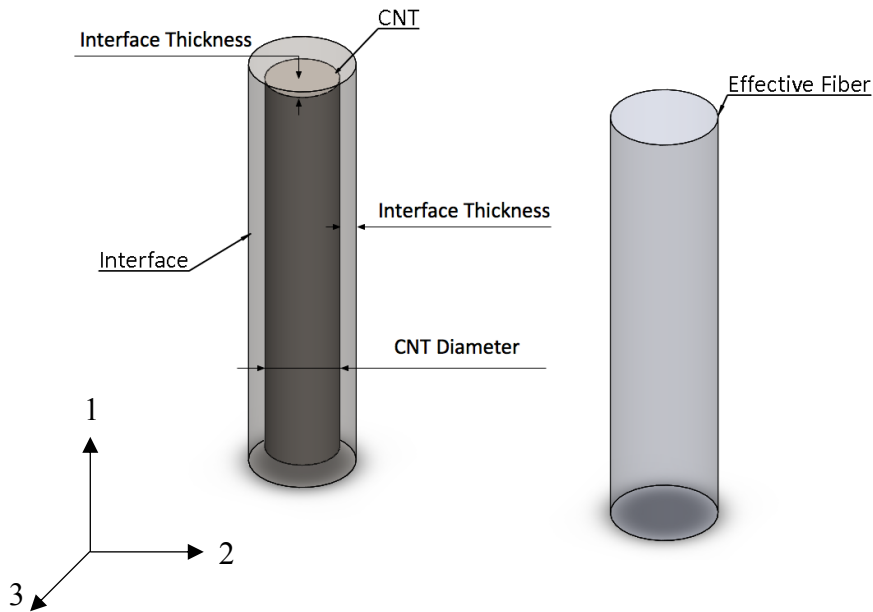


Figure 9: Isometric views of finite element models consisting of CNT and the interface (left), and effective fiber (right).

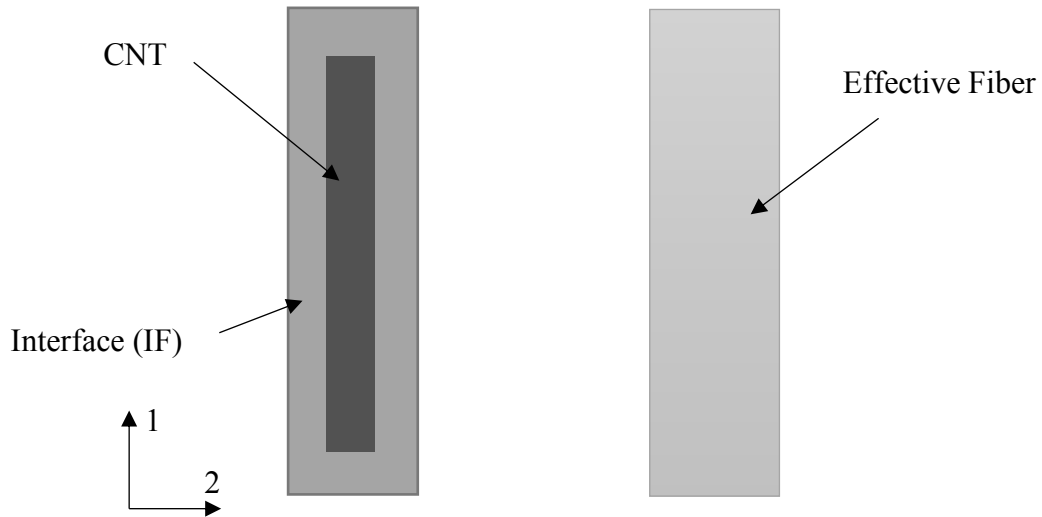


Figure 10. Side views of finite element models consisting of CNT and the interface (left), and effective fiber (right).

The two finite element models have identical outer dimensions. We used Abaqus FEA to build the models consisting of C3D10 elements. Approximately 22000 elements were used for the CNT-interface model and 70000 elements for the effective fiber model. A study was performed on the convergence of the solutions and it was verified that the numbers of elements used were sufficient.

The effective fiber is expected to show transversely isotropic behavior, resembling the CNT. A transversely isotropic material has 5 independent material properties that we have to determine before using the effective fiber in the micromechanical model. While a number of combinations can be listed for the 5 independent parameters, we decided to use longitudinal and transverse Young's moduli, E_1 and E_2 , shear modulus G_{12} and Poisson's ratios ν_{12} and ν_{23} . All the other moduli can be calculated using these 5 parameters assuming the effective fiber is transversely isotropic.

With the addition of the effective fiber the sequence of operations of the model is shown in Figure 11. Here "Micromechanics module" refers to Figure 7.

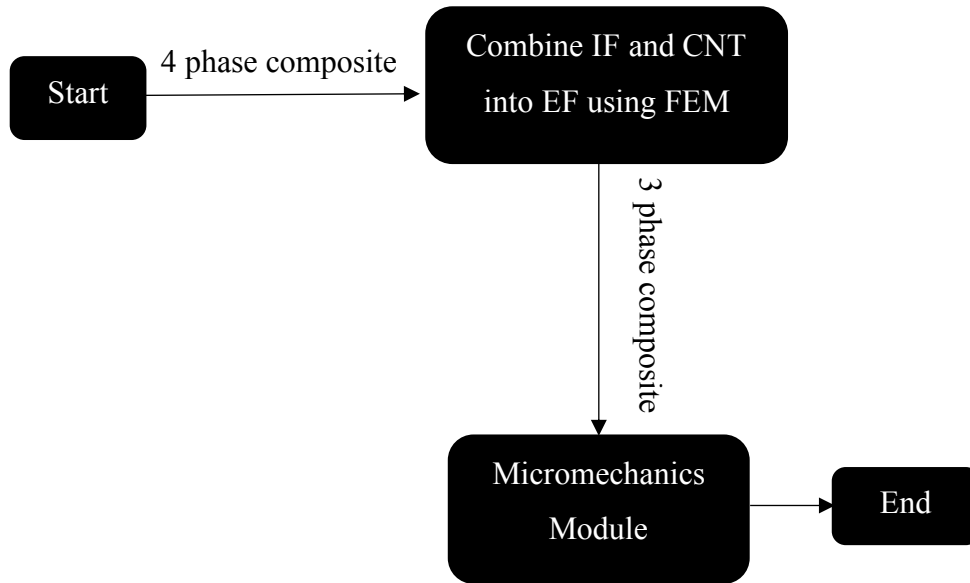


Figure 11: Sequence of operations in the current model.

2.4.3.1 Young's Modulus E_1 in the Longitudinal Direction

In order to obtain the Young's modulus in the longitudinal direction we applied uniform pressure on one end of the finite element models and assumed the other end is symmetric in the longitudinal direction. This is tantamount to making the cylinders twice as long and applying the same uniform pressure on both ends. The average displacement in the surface with applied pressure is then used as a measure of comparison between the two sets of finite element models.

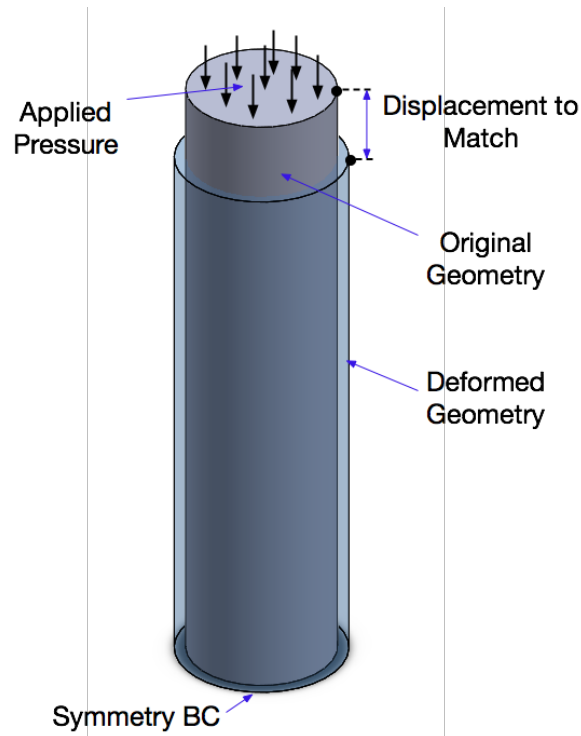


Figure 12: Loading conditions used to obtain the longitudinal modulus of the effective fiber.

2.4.3.2 Young's Modulus E_2 in the Transverse Direction and Poisson's ratio ν_{12}

The next two coefficients, E_2 and ν_{12} can be determined in the same loading by measuring and matching the displacements in different directions. To this end we loaded the finite element model with a uniform pressure on the sides as shown in Figure 13. Then the average displacement of the top surface in the longitudinal direction, as well as the average shrinkage in the radius of the cylinder were used to determine the two elastic moduli.

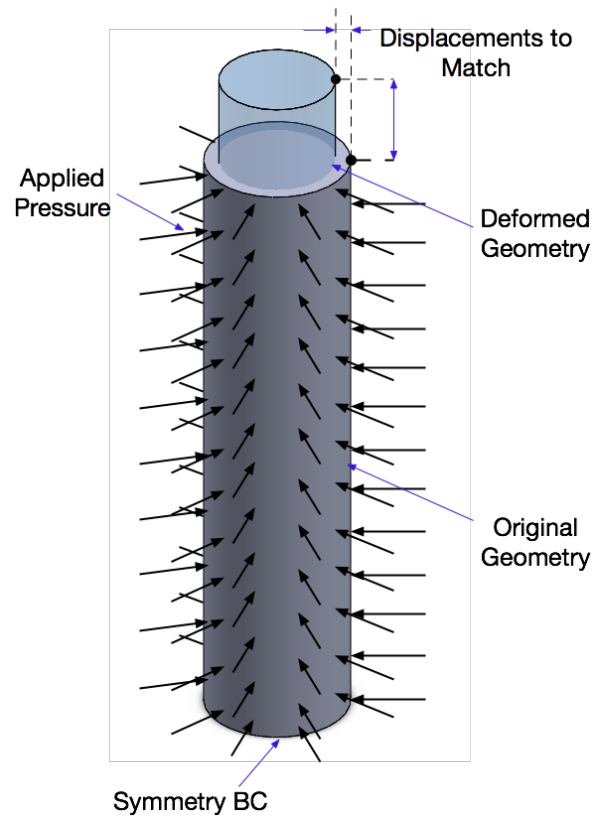


Figure 13: Loading conditions used to obtain the transverse modulus and Poisson's ratio ν_{12} of the effective fiber.

2.4.3.3 Shear Modulus G_{12} and Poisson's ratio ν_{23}

Out-of-plane shear modulus G_{12} and the associated Poisson's ratio ν_{23} are calculated next. For this purpose, the finite element model was twisted on one end with a uniformly distributed torsional load while the other end was assumed to have a symmetric boundary condition as shown in Figure 14. The average radial displacement on the top surface was then taken as the criteria to determine the shear modulus.

It was observed that the Poisson's ratio ν_{23} did not affect the results in any of the loading conditions used so far in a discernable way. This not only implies that the methods used so far cannot be used to determine this coefficient, but also that it does not significantly alter the results. While a new methodology could be devised to determine ν_{23} the fact that it does not alter the results a lot suggested that a simple assumption for this parameter could suffice. This practice is common for this coefficient in the literature [24]. To this end we assumed two values for ν_{23} ; 0.2 and 0.4 and observed that the moduli of the nanocomposite were not affected in a distinguishable way.

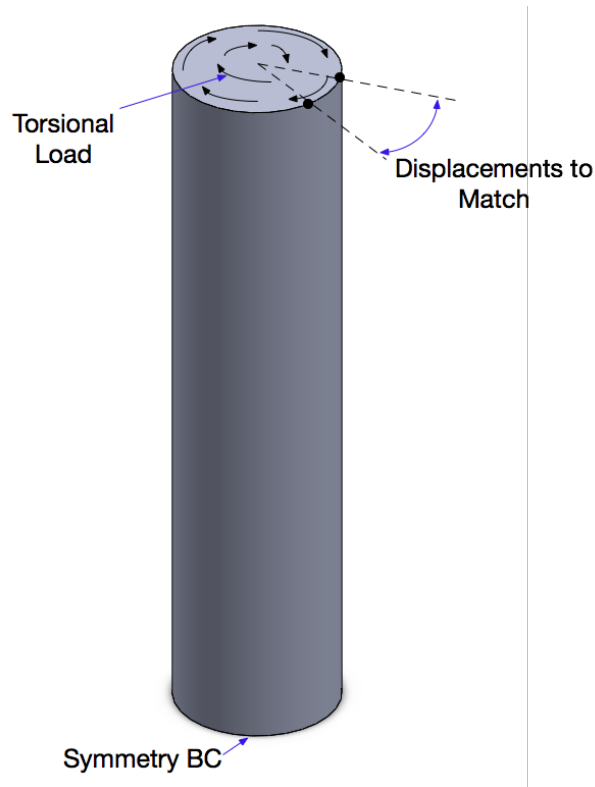


Figure 14: Loading conditions used to obtain G_{12} .

The elastic moduli were then obtained using the methodology described so far. The results are shown in Table 2 for the stiff interface model and Table 3 for the soft interface model.

Table 2: Transverse elastic constants of the effective fiber with a stiff interface model ($E_{IF} = 5 E_{polymer}$)

CNT Radius [Å]	E_1 [GPa]	E_2 [GPa]	G_{12} [GPa]	ν_{12} [-]	ν_{23} [-]
3.9	113.0	38.0	40.0	0.32	0.2
5.5	112.0	19.6	49.0	0.32	0.2
7.1	73.2	17.0	39.0	0.34	0.2

Table 3: Transverse elastic constants of the effective fiber with a soft interface model ($E_{IF} = 0.3 E_{polymer}$)

CNT Radius [Å]	E_1 [GPa]	E_2 [GPa]	G_{12} [GPa]	ν_{12} [-]	ν_{23} [-]
3.9	14.7	3.81	4.5	0.33	0.2
5.5	14.0	2.01	3.8	0.6	0.2
7.1	13.2	1.84	2.8	0.9	0.2

Detailed information about effective fiber property determination is given in Appendix C.

2.4.3.4 Verification with a Rheological Model

The elastic moduli obtained above for the effective fiber region can be verified using a simple springs analogy for a quick sanity check. For this purpose, the CNT and interface combination is divided into four regions consisting of

1. CNT
2. Portion of the interface covering the sides of the CNT
3. Portion of the interface covering the top of the CNT
4. Portion of the interface covering the bottom of the CNT

The four regions are shown in Figure 15

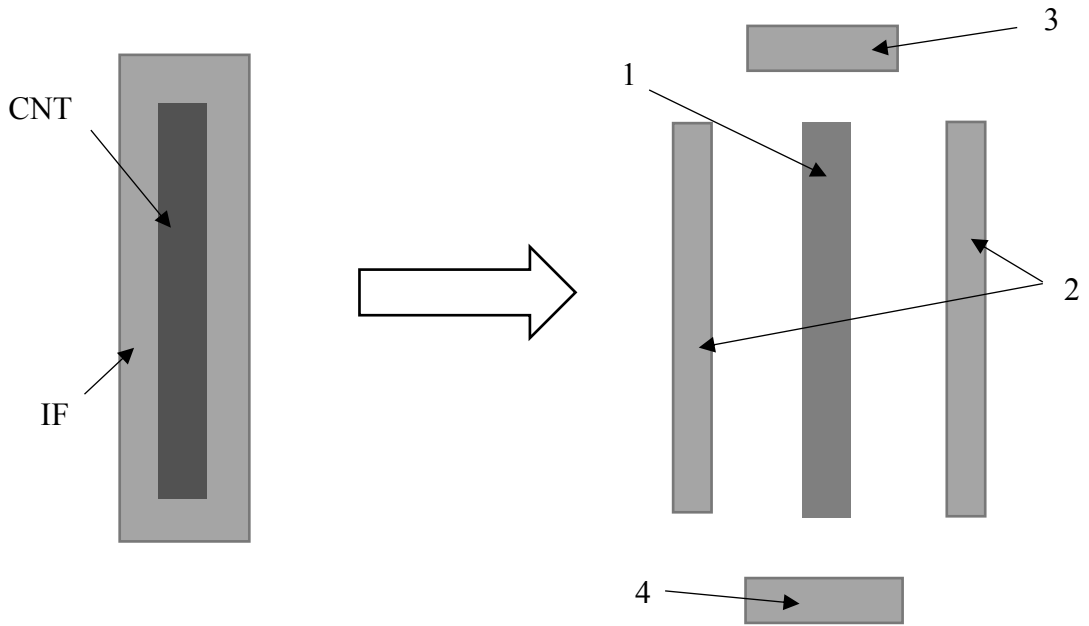


Figure 15. Partitioning of the CNT and interface model into four regions.

Idealizing the four regions as simple beams and modifying Hooke's law we can replace the 4 regions by simple springs. Hooke's law for simple beams in uniaxial loading reads

$$\begin{aligned}
 \sigma &= E\epsilon \\
 \frac{F}{A} &= E \frac{x}{L} \\
 F &= \frac{EA}{L} x
 \end{aligned}
 \tag{28}$$

where F represents the applied force, E its Young's modulus, A its cross sectional area, L its length and x its elongation. The last expression in Eqs. (28) is identical to the constitutive equation of a simple string, i.e. $F = kx$. Then the structural elements can be replaced with springs that have spring constants that are equal to $k = \frac{EA}{L}$.

The four regions can then be represented by simple springs with effective stiffnesses k_1, k_2 and $k_3 = k_4$ as shown in Figure 16.

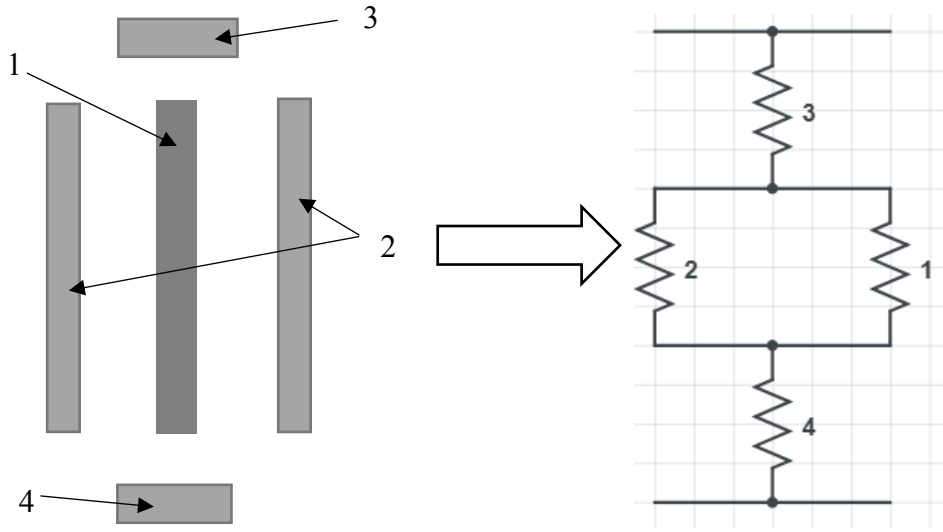


Figure 16. Simplification of the 4 regions in the CNT + interface model with linear springs.

$$k_i = \frac{E_i A_i}{L_i} \quad (29)$$

Then the effective fiber of the whole model is obtained using equations for the effective spring constants of springs connected in series and parallel as follows:

$$k = k_2 + \frac{k_1 k_3}{2k_1 + k_3} \quad (30)$$

$$E = \frac{kL}{A}$$

Using this method yields the following values for the longitudinal Young's modulus of the effective fiber:

Table 4: Longitudinal Young's modulus of the effective fiber for the three CNT radii and the stiff interface model calculated with the rheological model.

CNT Radius [Å]	E_1 [GPa]
3.9	162.4
5.5	159.1
7.1	154.4

Table 5: Longitudinal Young's modulus of the effective fiber for the three CNT radii and the soft interface model calculated with the rheological model.

CNT Radius [Å]	E_1 [GPa]
3.9	15.0
5.5	15.0
7.1	14.9

Table 4 and Table 5 serve to verify the results of Table 2 and Table 3, respectively. Being highly simplified, the rheological model is bound to have some errors, which is seen from the comparison of Table 2 and Table 4. However, the results match much better when using a soft interface model.

2.4.4 Interphase (IP)

The interphase is a portion of the polymer that has altered properties next to the carbon nanotube. It has been observed that the density of the polymer rises quasi-exponentially with some oscillations in the direct vicinity of the nanotube in the radial direction [17,24]. For example in the density plot of Figure 17 generated by Tsai et al. [24] one can see the spike in density of the polymer (polyamide – PI) close to the surface of the CNT. This jump in the density corresponds to the interphase region, while the gap between the interphase and the CNT (indicated by a density of 0 g/cc) is the interface. This can also be seen in the atomistic simulations of Herasati et al. [37] reported in Figure 18.

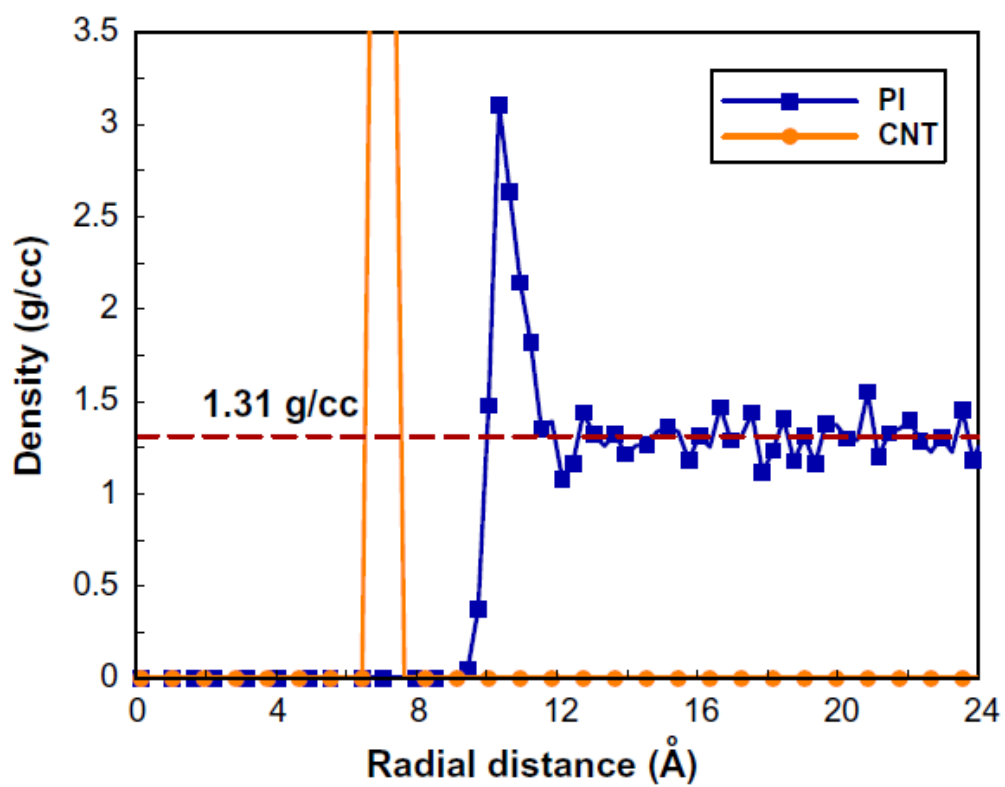


Figure 17. Density distribution of a PI-CNT composite in the radial direction originating in the center of the CNT. Image courtesy of [24].

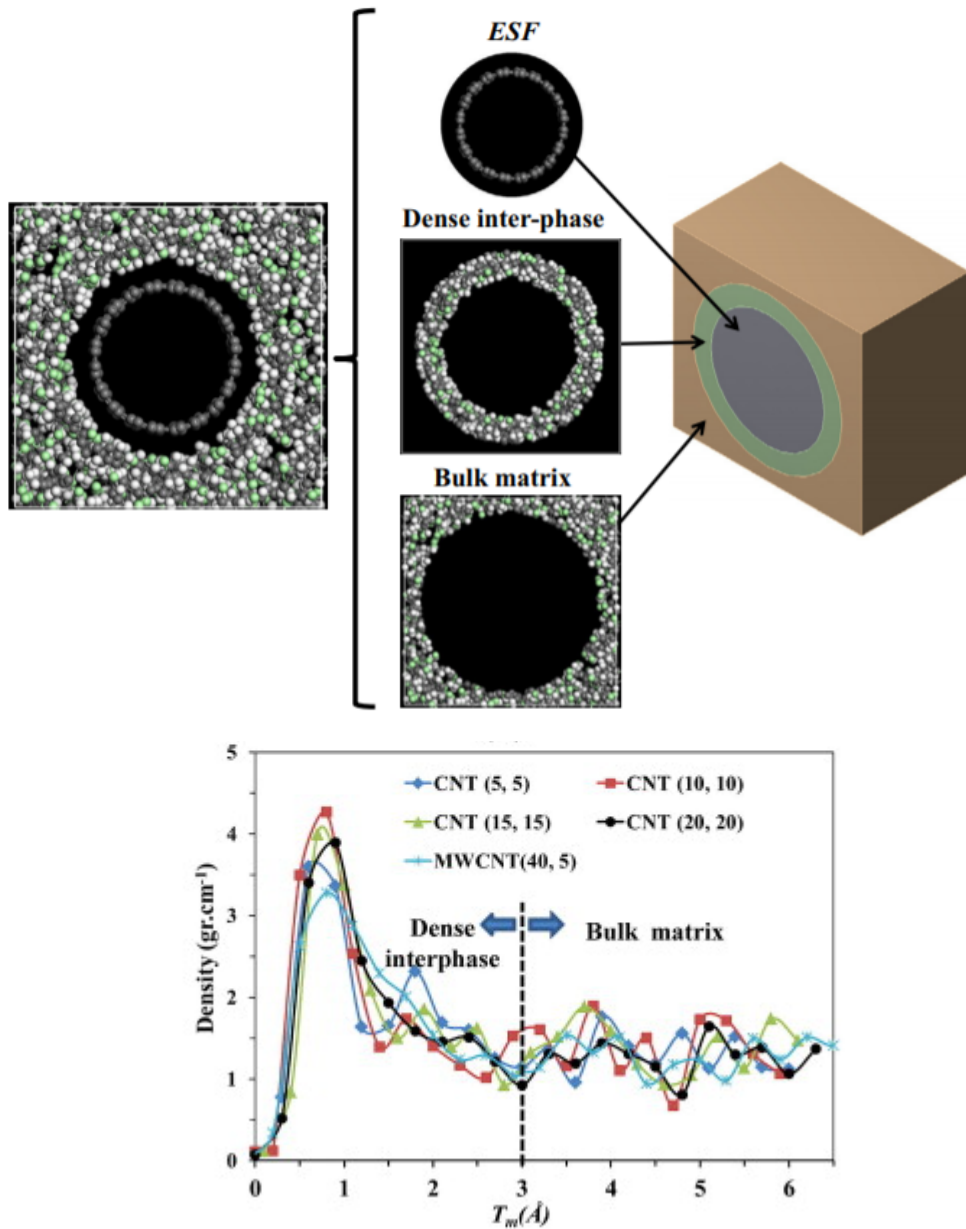


Figure 18. Atomistic images of the interphase region in a Poly Vinyl Chloride (PVC)–CNT Composite (top) and density distribution of Poly Vinyl Chloride (PVC) in the radial direction from surface of the CNT (bottom). Image obtained from [37].

This suggests a functionally graded model could better represent the true nature of the interphase. We chose three functions to model the interphase; constant, linear and exponential. The exponential function is given as

$$E(x) = \frac{E^{(2)} - E^{(1)}}{e^{-a} - 1} (e^{-ax} - 1) + E^{(1)} \quad (31)$$

where $x = 0$ and $E = E^{(1)}$ at the inner boundary (next to the interface) and $x = 1$ and $E = E^{(2)}$ at the outer boundary of the interphase. a is a parameter that controls the rate of exponential decay. Moduli $E^{(1)}$ and $E^{(2)}$ can be chosen to be equal to anything depending on the situation. In the current study, it was deemed necessary that when an effective fiber is used to replace the interface and the CNT the Young's modulus be continuous, such that the Young's modulus at the inner boundary is equal to the longitudinal Young's modulus of the effective fiber, $E^{(1)} = E_{EF}$. The modulus at the outer boundary is then set to be equal to that of the bulk polymer, $E^{(2)} = E_{BP}$. Poisson's ratio of the interphase was kept constant and equal to that of the polymer. The thickness of the interphase is an important parameter; however, its value is highly controversial. Interphase thickness values ranging from 3 to 25.5 Å have been reported in the literature [17,24,38].

Figure 19 shows the distribution of the Young's modulus across the whole composite in a figurative manner when an effective fiber is used instead of the CNT and the interface.

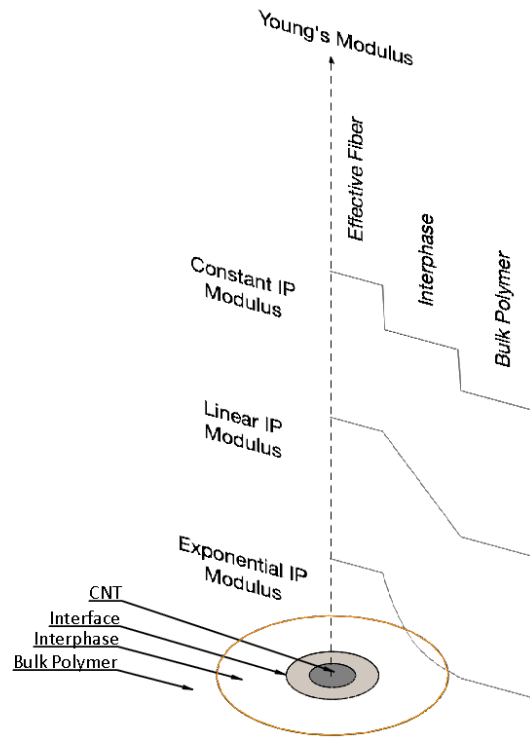


Figure 19: Representative Young's modulus distribution across the micromechanical model. This representation of the interphase is in line with the observations made in experiments of nanoparticulate composites as shown in Figure 20 and Figure 21.

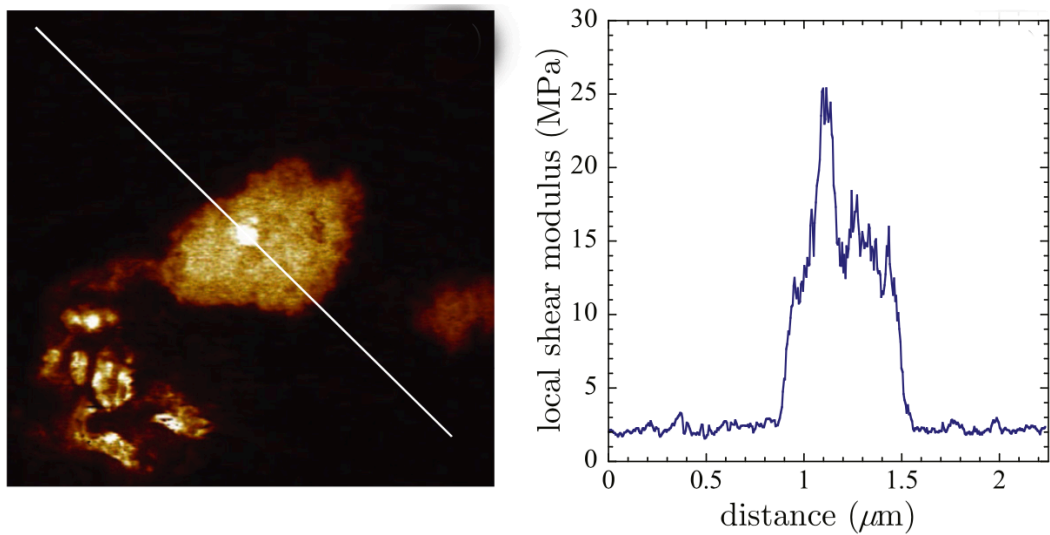


Figure 20. Illustrated AFM measurement of the local shear modulus around a TiO_2 -Elastomer nanocomposite. Note that the abscissa of the plot on the right side corresponds to the white line crossing the nanoparticle on the left side. Image obtained from [39].

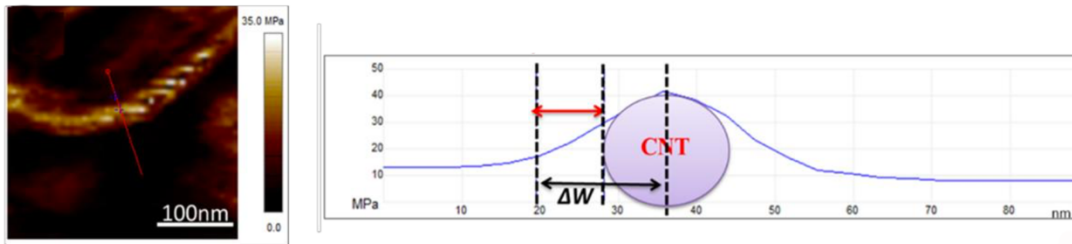


Figure 21. Representative Young's modulus of CNT-Natural Rubber nanocomposite and its corresponding modulus-length curve to represent the interphase thickness. Image obtained from [40].

2.4.5 Bulk Polymer (BP)

In this study, the resulting moduli of the nanocomposite are studied relative to that of the polymer using stiffening ratios. As such the absolute values of the polymer moduli were not held in high significance. But it was deemed beneficial to use a polymer from which a carbon nanotube composite has previously been synthesized. To this end a polymer named LARC-SI produced and tested by [14] is used that has a Young's modulus of 3.8 GPa and a Poisson's ratio of 0.4.

CHAPTER 3

RESULTS AND DISCUSSION

3.1 Results

A LARC-SI – SWCNT polymer was then analysed using the micromechanical model described in CHAPTER 2. A number of parametric studies were performed to study the effects of various variables such as the number of inclusions, interphase thickness, CNT radius and et cetera on the moduli of the composite. In all of these studies the orientation distribution of the carbon nanotubes was assumed to be random, unless specified otherwise. The results were compared with other numerical as well as experimental studies in the literature whenever possible.

3.1.1 Number of Inclusions

One of the most fundamental methods that can be used to model carbon nanotube – polymer composites is that of Mori and Tanaka [20] using two phases. However, as described in the previous chapter this is very unrealistic. It is widely known that there are at least four phases in a nanocomposite that should be accounted for in the micromechanical model. In this subsection, we study how reducing the number of inclusions to 3 or even 2 affects the performance of the micromechanical model. We use three micromechanical models consisting of a two-phase Mori-Tanaka model, a 3-phase and a 4-phase model and compare the moduli resulted by the three models. In the 2-phase model the two phases consist of a CNT phase and a polymer phase, while the existence of other phases is ignored. In the 3-phase model the three phases are the CNT, interface and the polymer, while the interphase is assumed not to exist. Finally, in the 4-phase model all the four phases are present. The moduli of the phases are

described in CHAPTER 2. In all three cases the polymer, interface, and CNT are used as described in 2.4.3 Effective Fiber (EF), 2.4.2 Interface (IF) (assuming a stiff interface) and Table 1 respectively. In the 4 phase model the interphase moduli are assumed to vary from those of the interface and the polymer respectively. We do not use an effective fiber in this subsection to keep the results simple, but we still apply randomization of CNT orientation distribution.

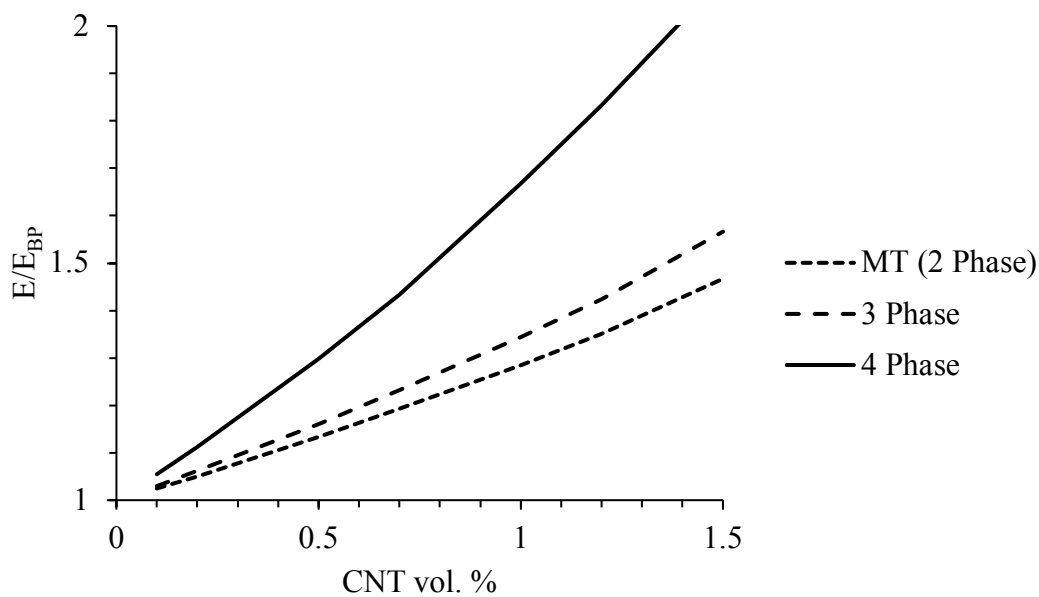


Figure 22. Comparison of 2-phase, 3-phase and 4-phase micromechanical models.

The results of the analysis are shown in Figure 22. Only Young's modulus is shown to keep the figure simple, but shear modulus follows a similar trend as a result of homogenization of the CNT orientation distribution. Note that an exponential interphase modulus distribution was used with $\alpha = 5$, CNT radius of 3.9 \AA , interphase thickness of $t_{IP} = 10 \text{ \AA}$ and a CNT aspect ratio of 40. The 4-phase model currently overestimates the moduli of the composite because the micromechanical model does not "see" that the interface is coated around the CNT. In reality the CNT does not interact with the polymer directly, and instead, stresses are transferred to the CNT through the interface. However, as the purpose of this model is to show how the

number of phases affects the results, the current configuration is deemed to be sufficient and the issue of “coating” of the interface is considered in the next subsections. It is also beneficial as using a coated effective fiber model would cause a negative effect on the moduli of the composite which would bring it closer to the other two models in Figure 22 thus obscuring the error caused by the other two methods. The modulus of the interphase is supposed to start from that of the interface and end with that of the polymer.

3.1.2 Interphase Modulus Distribution

The interphase is a crucial phase in the nanocomposite. According to some theories the entirety of the stiffening effect of the carbon nanotube is due to the interphase, rather than the direct contribution of the CNT [17]. Even if this is not the case, depending on the size of the interphase it could have a large effect on the stiffness of the composite. Even using moderate assumptions for interphase thickness such as 10 Å results in an interphase larger than the CNT and the interface combined. As such, it is of grave importance that the interphase be functionally graded. However, the nature of the function by which it is graded is an unknown. To study the effect of the function we plotted the normalized Young’s modulus of the nanocomposite for various CNT radii using different interphase modulus distribution functions in Figure 23. An interphase thickness of 10 Å and a volume fraction of 1% were assumed in this plot. For constant IP case the Young’s modulus of the IP was set to the average of the longitudinal Young’s modulus of the effective fiber and Young’s modulus of the polymer.

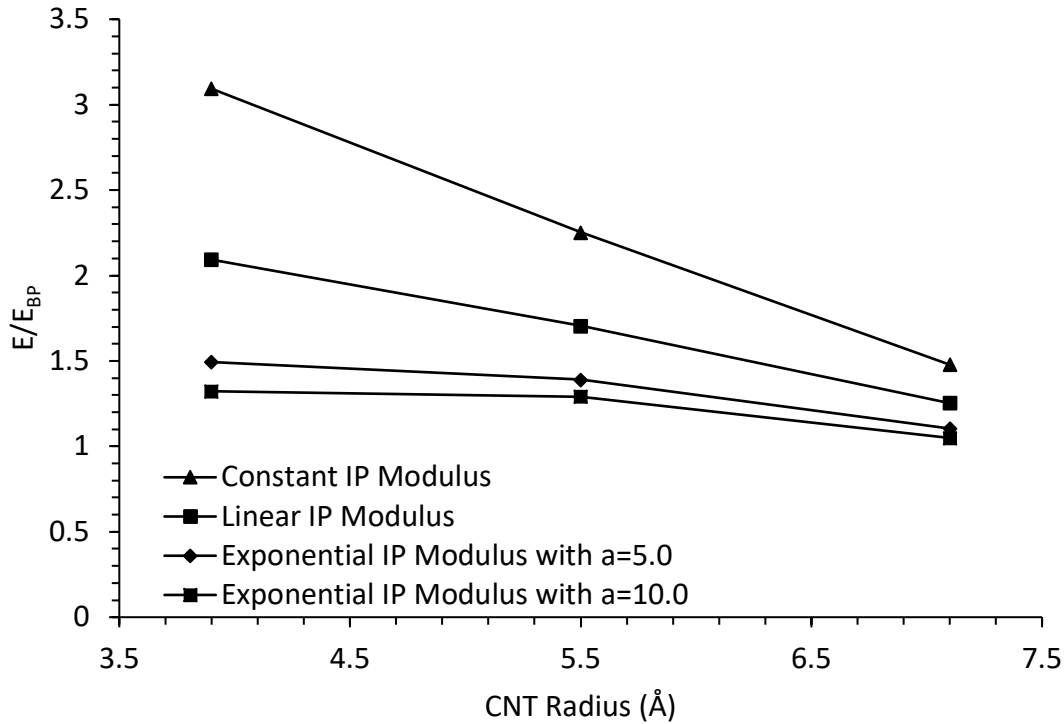


Figure 23. Normalized composite moduli vs CNT radius for various interphase moduli distributions.

It is seen that the stiffening effect of the nanotube reduces as its radius grows. This is an expected behavior with multiple reasons. First, since the CNTs used in this study are single walled, a larger CNT means a larger empty space inside the CNT. The only part of the CNT that contributes to the stiffness is the part with carbon atoms, known as the wall. But a larger CNT radius means a smaller portion of the CNT is occupied by the wall; resulting in reduced CNT moduli.

Furthermore, keeping the volume fraction of the inclusion the same but increasing the CNT radius effectively means reducing the number of carbon nanotubes in the composite, but increasing their size. Since the thickness of the interphase is constant with respect to CNT radius [17], and since the interphase also has a great stiffening effect on the composite, using smaller but more numerous carbon nanotubes result in more of the polymer being turned into the interphase.

Figure 23 also shows how choosing different functions for the distribution of the Young's modulus in the interphase affects the stiffness of the nanocomposite. It is

observed that using a constant and linear distribution results in unreasonably large and unrealistic stiffening ratios. For example, using 1% CNT by volume with a radius of 3.9 Å and a constant interphase modulus distribution results in a composite stiffness that is more than 3 times that of the polymer.

An exponential distribution is also much more flexible than the other two distributions with the parameter a . One can even simulate constant and linear distribution by utilizing proper values of a . Last but not least the use of an exponential distribution is further motivated by the observations made in the literature that the density of the interphase shows a quasi-exponential decay with some oscillations in the radially outward direction from the center of the CNT [17,24,27].

3.1.3 Contributions of the Phases

Figure 24 and Figure 25 show column charts of the contribution of each phase to the stiffness of the nanocomposite when using stiff and soft interface models respectively. These plots were obtained by starting from a pure polymer and gradually adding the rest of the phases in correct volume fractions. The volume fraction of the CNT was kept at 1% and radius at 3.9 Å. This plot serves to show three important concepts. First, one can clearly see that all four phases in the nanocomposite are contributing in significant proportions to the modulus using a stiff interface. On the other hand, using a soft interface degrades the stress transfer mechanism to the point that the interface and the CNT play almost no role in the reinforcement of the polymer. A similar study was previously obtained in [17]. However, it should be noted that the interphase profile was kept constant in both cases. This is seen as an explanation, and thereby justification, of the use of the current 4-phase model.

One can also see that the interphase becomes increasingly important as its thickness grows to even mediocre values. At an interphase thickness of 10 Å the interphase occupies more volume than the CNT and reinforces the polymer almost as much as the CNT.

Last but not least the plot shows how the interface really works. The plot has three sets of columns, the left one in each set represents the coated inclusion model with effective

fiber. The right one represents a classical Mori-Tanaka type model with 4 phases. As discussed in 2.4.3 Effective Fiber (EF) the Mori-Tanaka type model does not consider the coated nature of the phases. And since the interface has a higher stiffness than the polymer, the model predicts that the interface has a positive contribution to the stiffness of the nanocomposite (shown in light gray in Figure 24). While in reality the opposite is true. The interface serves to weaken the carbon nanotube resulting in a negative contribution to the stiffness of the nanocomposite. The real contribution of the interface is the difference between the contributions of the carbon nanotubes and effective fibers in each set which is only evident when a coated interface model is utilized. In other words, using a purely micromechanical model does not fully disclose the role of the interface in the nanocomposite. Since the interface is such a small phase, its direct contribution to the nanocomposite is not very significant. This is evident from the fact that the right columns in the two figures are almost identical. This issue however, is tackled by the homogenization of the CNT and the interfaces using finite element analyses (See the difference in the left columns).

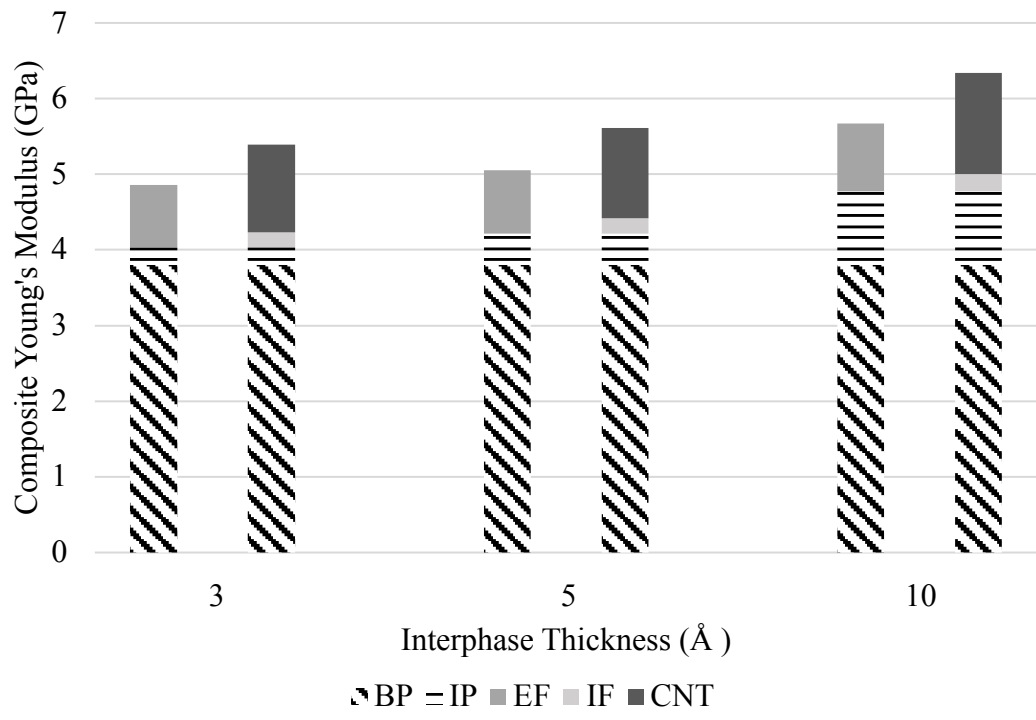


Figure 24. Contribution of each phase to the modulus of the nanocomposite when using a stiff interface model.

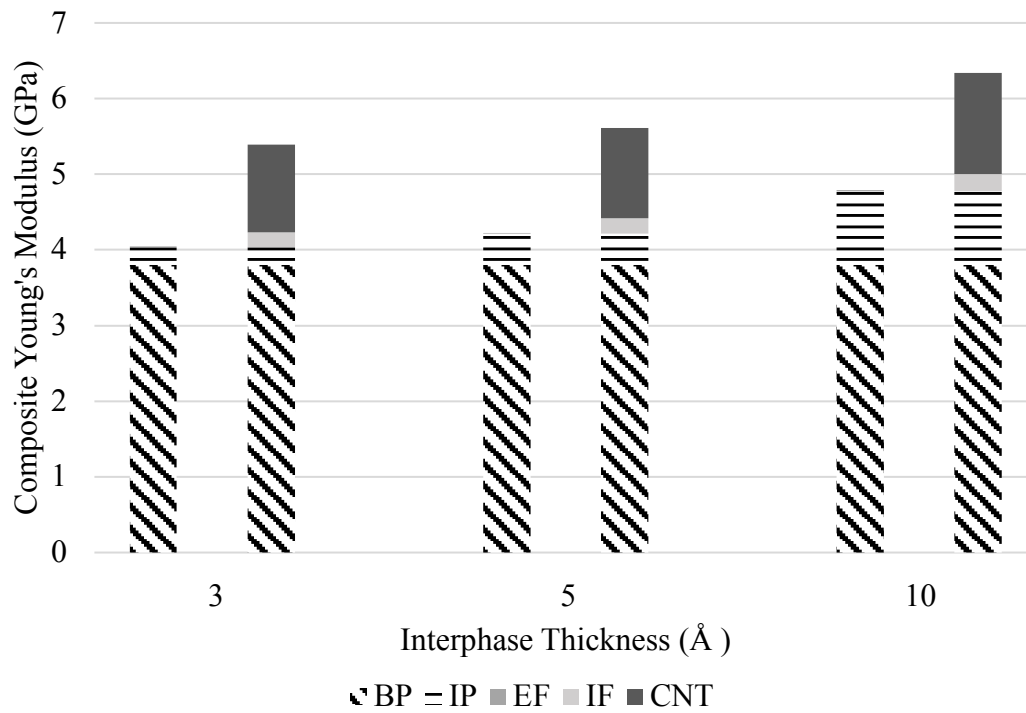


Figure 25. Contribution of each phase to the modulus of the nanocomposite when using a soft interface model.

3.1.4 Interphase Thickness

Since the interphase seems to carry arguably the greatest role in the stiffening of the nanocomposite, it is important to characterize and study the interphase as much as possible. The most controversial aspect of the interphase is probably its thickness. Figure 26 shows the variation of normalized composite stiffness as a function of CNT vol. %. Some other numerical and experimental data is also superimposed to compare the current model with the findings in the literature [14,41,42]. The plot was obtained using $a = 5$. The plot indicates that increasing CNT volume fraction exponentially increases the stiffening ratio.

It is observed that the current model overestimates the composite stiffness especially in increasing volume fractions. This is because as the volume fraction increases the micromechanical model approaches the dilute limit. The model also does not take into

effect issues such as proper dispersion and distribution of CNTs across the composite, which get worse with increasing volume fractions.

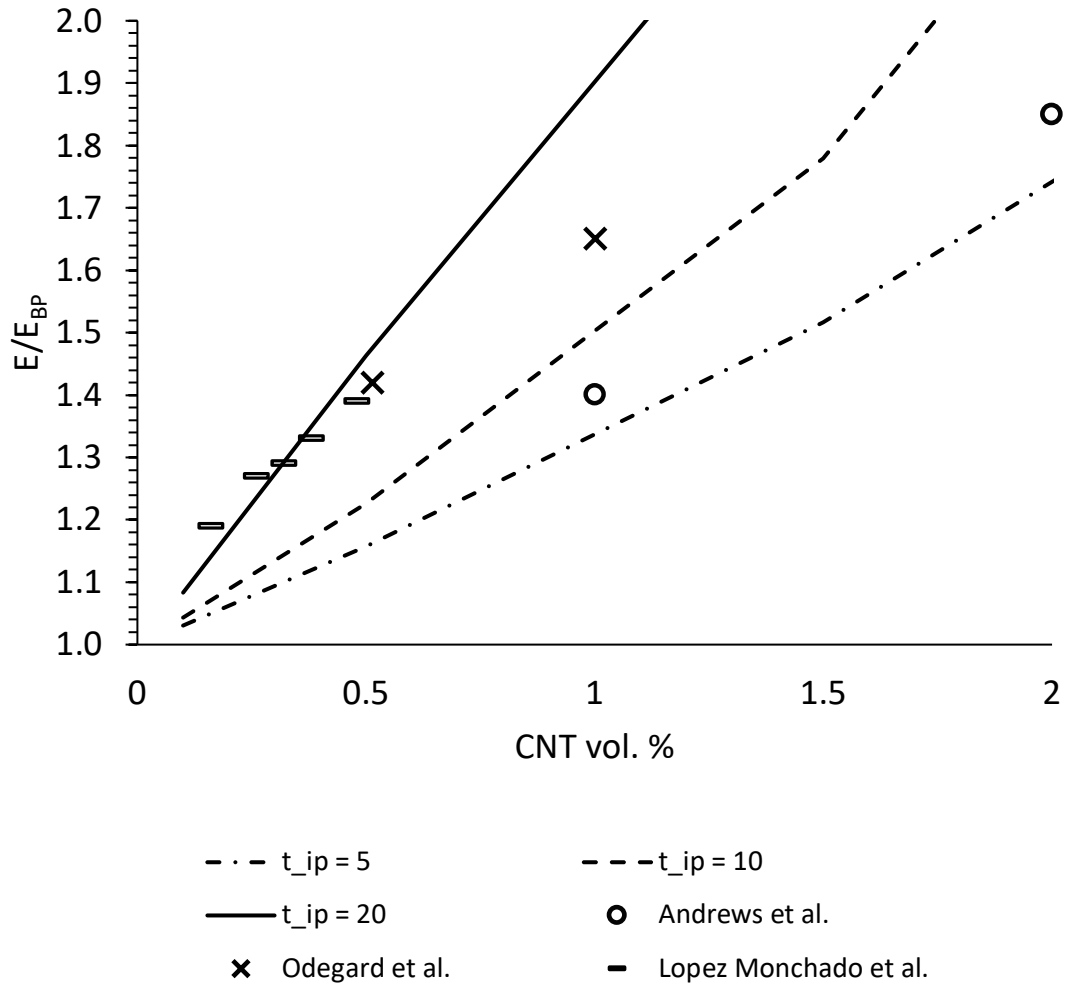


Figure 26. Results of the current model using a CNT radius of 3.9 Å, interphase thickness of 3 Å, and $a = 5$ compared to experimental and numerical findings in the literature [14,41,42].

3.1.5 CNT Orientation Distribution

The analyses performed so far assumed a random distribution of CNT orientation in the composite. This assumption leads to isotropic composites. However, if for some reason the distribution is not random an anisotropic composite is obtained. For example, if the fibers tend to align towards a single direction the composite becomes

stiffer in that direction and softer in others. In Figure 27 two sets of composite moduli are plotted that were obtained using random and completely aligned distributions of CNT orientation. An interphase thickness of 5 Å and $a = 1$ are used. It is seen that the Young's modulus of the aligned composite in the direction of alignment, 1, is very high, while shear modulus and Young's modulus in the transverse direction are lower. On the other hand, a random distribution of CNT orientation results in both moduli (shear and Young's) with moderate values.

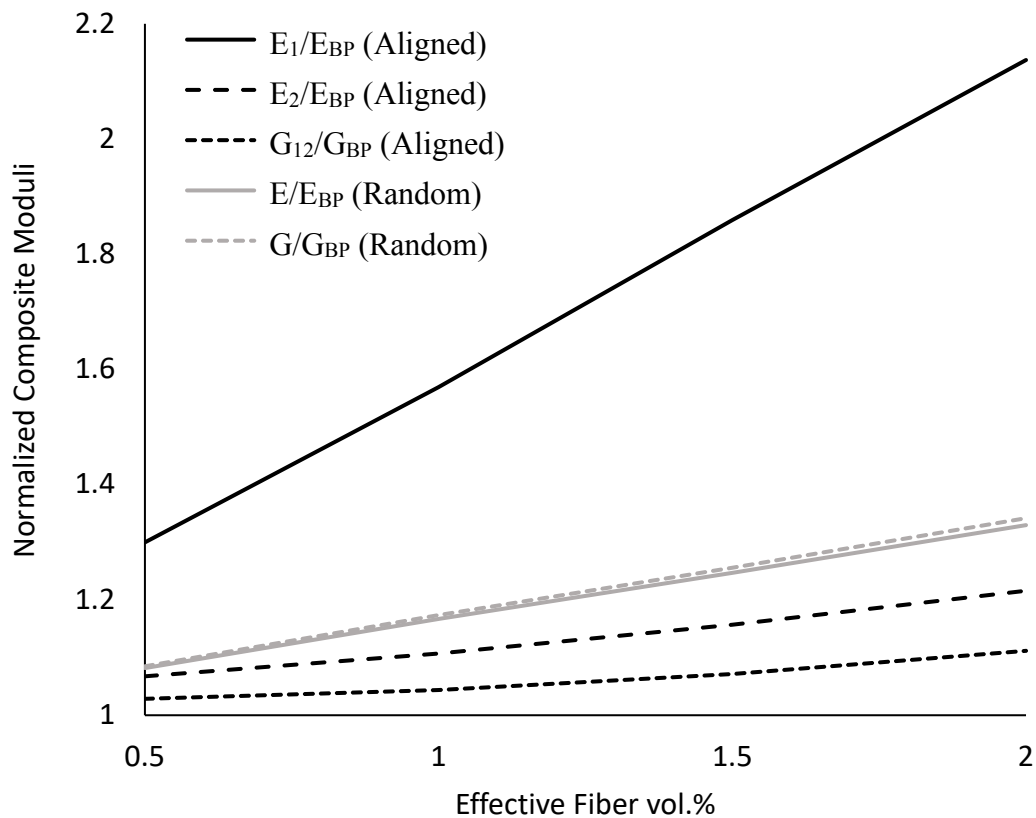


Figure 27: Composite moduli vs effective fiber vol.% for aligned and random inclusion distributions.

3.1.6 CNT Aspect Ratio

Aspect ratio of the CNT is defined as the ratio of its length to its width. A CNT with a relatively higher aspect ratio results in higher stiffness. This is because a CNT with higher aspect ratio has a greater contact area with the polymer, resulting in better adhesion. However, the adhesion properties saturate when a certain aspect ratio is

reached. Figure 28 shows a plot of normalized CNT moduli as a function of effective fiber aspect ratio. The data plotted indicates that the moduli rise sharply until an aspect ratio of about 20, and some more until 50, but after that no discernable change is seen as a function of aspect ratio. The data plotted was obtained for CNT radius of 3.9 Å and 1% effective fiber by volume.

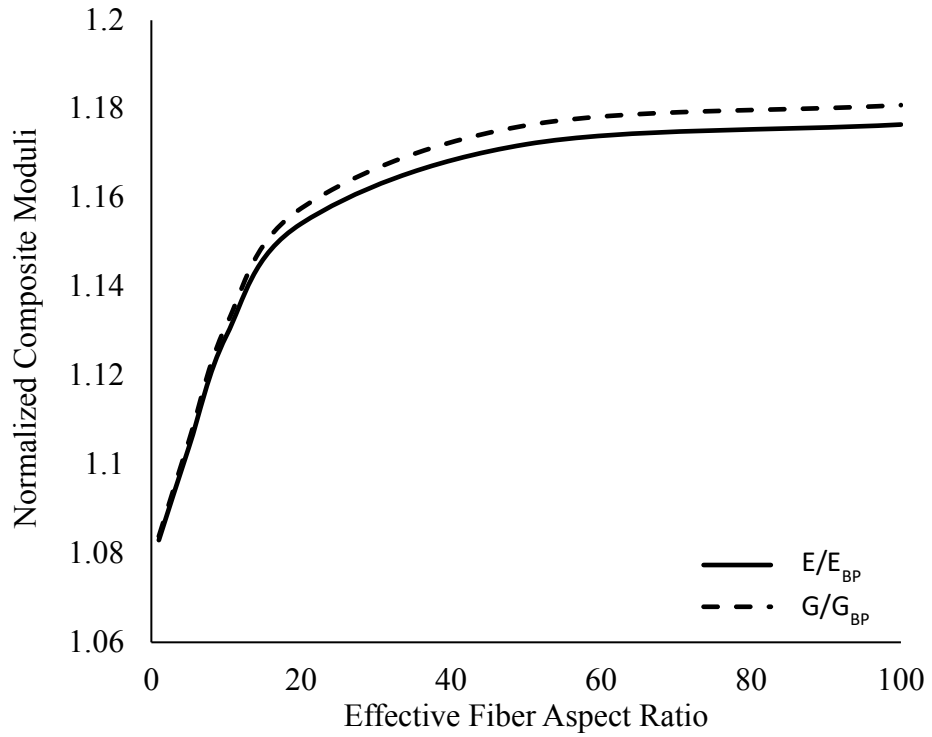


Figure 28: Composite Young's and shear moduli vs effective fiber aspect ratio

CHAPTER 4

CONCLUSIONS

Numerous molecular dynamics studies reported in the literature indicate that there are at least four distinct regions, or phases, in a carbon nanotube – polymer nanocomposite including the carbon nanotube, the interface, the interphase and the bulk polymer. Since the phases have highly varying roles and mechanical properties, it is important to account for all of them when developing a model for nanocomposite simulation.

The interface is a small and soft region dominated by Van der Waals bonds, as compared to the covalent bonds of the carbon nanotube, and it is mainly responsible for stress transfer from the polymer to the CNT. Since Mori-Tanaka based models do not take into account this property, it is important to model this region with a different method such as the finite element method so that the true role of the interface is accounted for.

It is also noted that as opposed to the commonly held notion in the literature, the CNT is not the only stiffening agent in the nanocomposite. In fact, the interphase may be even more important than the CNT in this regard. Since the interphase consists of such a large swathe of the nanocomposite it has a crucial effect on the stiffness of the composite.

This study shows that carbon nanotube – polymer nanocomposites can be modelled with high fidelity using 4 phases and properly integrating the phases in a way which accurately reflects the true nature of the phases in an actual nanocomposite.

4.1 Recommendations and Future Work

It is observed during the course of this study that some experimental and atomistic scale studies are required to better understand CNT-polymer composites. For example, there is no single, or even converging, point of view on the thickness of the interphase in the literature. This is despite the fact that the interphase probably has the greatest impact in stiffening of the nanocomposite. Studies focusing on the thickness of the interphase and its dependencies on various outside parameters could highly improve the state of the analytical models currently available.

The moduli tensor of the CNT and the interface change with CNT radius. The way in which this change occurs is of crucial importance in modeling of nanocomposites. If the evolution of the moduli of the CNT with its radius, as well as the number of walls and chirality vectors is better understood, this could lead to ever self-sustaining methods to be developed for the simulation of carbon nanotube composites.

In terms of modeling it is advised that a multitude of methodologies be used in harmony, as was done in this study, as it suits the challenges at hand. It is also possible that more compact methods such as Qu's micromechanical model introduced in CHAPTER 1 be used to simplify the models even more. However, a small loss in accuracy and fidelity is to be expected.

REFERENCES

- [1] S. Iijima, Helical microtubules of graphitic carbon, *Nature*. 354 (1991) 56–58.
- [2] R. Bacon, Growth, structure, and properties of graphite whiskers, *J. Appl. Phys.* 31 (1960). doi:10.1063/1.1735559.
- [3] O. Kanoun, C. Müller, A. Benchirouf, A. Sanli, T.N. Dinh, A. Al-Hamry, L. Bu, C. Gerlach, A. Bouhamed, Flexible carbon nanotube films for high performance strain sensors., *Sensors (Basel)*. (2014). doi:10.3390/s140610042.
- [4] M. Loos, *Carbon Nanotube Reinforced Composites*, 1st ed., William Andrew, Waltham, 2015.
- [5] C.M.L. Eric W. Wong, Paul E. Sheehan, Nanobeam Mechanics: Elasticity, Strength, and Toughness of Nanorods and Nanotubes, *Science (80-.)*. 277 (1997) 1971–1975. doi:10.1126/science.277.5334.1971.
- [6] A. Krishnan, E. Dujardin, T.W. Ebbesen, P.N. Yianilos, M.M.J. Treacy, Young’s modulus of single-walled nanotubes, *Phys. Rev. B*. 58 (1998) 13–19. doi:10.1103/PhysRevB.58.14013.
- [7] P.K. Aravind, The physics of the space elevator, *Am. J. Phys.* (2007). doi:10.1119/1.2404957.
- [8] K.I. Tserpes, P. Papanikos, Finite element modeling of single-walled carbon nanotubes, *Compos. Part B Eng.* 36 (2005) 468–477. doi:10.1016/j.compositesb.2004.10.003.
- [9] P. Papanikos, D.D. Nikolopoulos, K.I. Tserpes, Equivalent beams for carbon nanotubes, *Comput. Mater. Sci.* 43 (2008) 345–352. doi:10.1016/j.commatsci.2007.12.010.
- [10] S. Yang, S. Yu, W. Kyoung, D.S. Han, M. Cho, Multiscale modeling of size-dependent elastic properties of carbon nanotube/polymer nanocomposites with interfacial imperfections, *Polymer (Guildf)*. 53 (2012) 623–633. doi:10.1016/j.polymer.2011.11.052.
- [11] F.H. Gojny, M.H.G. Wichmann, U. Köpke, B. Fiedler, K. Schulte, Carbon nanotube-reinforced epoxy-composites: enhanced stiffness and fracture toughness at low nanotube content, *Compos. Sci. Technol.* 64 (2004) 2363–2371. doi:10.1016/j.compscitech.2004.04.002.
- [12] H. Meng, G.X. Sui, P.F. Fang, R. Yang, Effects of acid- and diamine-modified MWNTs on the mechanical properties and crystallization behavior

- of polyamide 6, *Polymer (Guildf)*. 49 (2008) 610–620.
doi:10.1016/j.polymer.2007.12.001.
- [13] J.N. Coleman, U. Khan, W.J. Blau, Y.K. Gun'ko, Small but strong: A review of the mechanical properties of carbon nanotube–polymer composites, *Carbon N. Y.* 44 (2006) 1624–1652. doi:10.1016/j.carbon.2006.02.038.
- [14] G.M. Odegard, T.S. Gates, K.E. Wise, C. Park, E.J. Siochi, Constitutive modeling of nanotube-reinforced polymer composites, *Compos. Sci. Technol.* 63 (2003) 1671–1687. doi:10.1016/S0266-3538(03)00063-0.
- [15] M. Cadek, J.N. Coleman, V. Barron, K. Hedicke, W.J. Blau, Morphological and mechanical properties of carbon-nanotube-reinforced semicrystalline and amorphous polymer composites, *Appl. Phys. Lett.* 81 (2002) 5123–5125. doi:10.1063/1.1533118.
- [16] D. Qian, E.C. Dickey, R. Andrews, T. Rantell, Load transfer and deformation mechanisms in carbon nanotube-polystyrene composites, *Appl. Phys. Lett.* 76 (2000) 2868. doi:10.1063/1.126500.
- [17] M. Malagù, M. Goudarzi, A. Lyulin, E. Benvenuti, A. Simone, Diameter-dependent elastic properties of carbon nanotube-polymer composites: Emergence of size effects from atomistic-scale simulations, *Compos. Part B Eng.* 131 (2017) 260–281. doi:10.1016/j.compositesb.2017.07.029.
- [18] J.D. Eshelby, The determination of the elastic field of an ellipsoidal inclusion and related problems, *Proc. R. Soc. A.* 241 (1957) 376–396. doi:10.1098/rspa.1957.0133.
- [19] J.D. Eshelby, Elastic Inclusions and Inhomogeneities, in: I.N. Sneddon, R. Hill (Eds.), *Prog. Solid Mech.*, 2nd ed., Physics Today, North Holland, Amsterdam, 1962: pp. 89–140. doi:10.1063/1.3058073.
- [20] T. Mori, K. Tanaka, Average stress in matrix and average elastic energy of materials with misfitting inclusions, *Acta Metall.* 21 (1973) 571–574. doi:10.1016/0001-6160(73)90064-3.
- [21] Y. Benveniste, A new approach to the application of Mori-Tanaka's theory in composite materials, *Mech. Mater.* 6 (1987) 147–157. doi:10.1016/0167-6636(87)90005-6.
- [22] J. Qu, Eshelby Tensor for an Elastic Inclusion with Slightly Weakened Interface, *J. Appl. Mech.* 60 (1993) 1048–1050.
- [23] S. Yang, M. Cho, A scale-bridging method for nanoparticulate polymer nanocomposites and their nondilute concentration effect, *Appl. Phys. Lett.* 94 (2009) 10–13. doi:10.1063/1.3143669.
- [24] J.L. Tsai, S.H. Tzeng, Y.T. Chiu, Characterizing elastic properties of carbon nanotubes/polyimide nanocomposites using multi-scale simulation, *Compos. Part B Eng.* 41 (2010) 106–115. doi:10.1016/j.compositesb.2009.06.003.
- [25] Z. Wang, R.J. Oelkers, K.C. Lee, F.T. Fisher, Annular Coated Inclusion

- model and applications for polymer nanocomposites – Part I: Spherical inclusions, *Mech. Mater.* 101 (2016) 170–184. doi:10.1016/j.mechmat.2016.07.004.
- [26] Z. Wang, R.J. Oelkers, K.C. Lee, F.T. Fisher, Annular Coated Inclusion model and applications for polymer nanocomposites – Part II: Cylindrical inclusions, *Mech. Mater.* 101 (2016) 50–60. doi:10.1016/j.mechmat.2016.07.005.
- [27] J. Choi, H. Shin, M. Cho, A multiscale mechanical model for the effective interphase of SWNT/epoxy nanocomposite, *Polymer (Guildf)*. 89 (2016) 159–171. doi:10.1016/j.polymer.2016.02.041.
- [28] J.Y. Li, Thermoelastic behavior of composites with functionally graded interphase: A multi-inclusion model, *Int. J. Solids Struct.* 37 (2000) 5579–5597. doi:10.1016/S0020-7683(99)00227-9.
- [29] M. Hori, S. Nemat-Nasser, Double-inclusion model and overall moduli of multi-phase composites, *Mech. Mater.* 14 (1993) 189–206. doi:10.1016/0167-6636(93)90066-Z.
- [30] N. Marzari, M. Ferrari, Textural and Micromorphological Effects on the Overall Elastic Response of Macroscopically Anisotropic Composites, *J. Appl. Mech.* 59 (1992) 269–275. doi:10.1115/1.2899516.
- [31] A.F. Ávila, S.G.R. Lacerda, Molecular Mechanics Applied to Single-Walled Carbon Nanotubes, *Mater. Res.* 11 (2008) 325–333. doi:10.1590/S1516-14392008000300016.
- [32] A.L. Kalamkarov, A. V Georgiades, S.K. Rokkam, Analytical and numerical techniques to predict carbon nanotubes properties, *Int. J. Solids Struct.* 43 (2006) 6832–6854. doi:10.1016/j.ijsolstr.2006.02.009.
- [33] C. Wei, D. Srivastava, K. Cho, Thermal Expansion and Diffusion Coefficients of Carbon Nanotube-Polymer Composites, *Nano Lett.* 2 (2002) 647–650. doi:10.1021/nl025554+.
- [34] L.S. Schadler, S.C. Giannaris, P.M. Ajayan, Load transfer in carbon nanotube epoxy composites, *Appl. Phys. Lett.* 73 (1998). doi:10.1063/1.122911.
- [35] P.M. Ajayan, L.S. Schadler, C. Giannaris, A. Rubio, Single-Walled Carbon Nanotube–Polymer Composites: Strength and Weakness, *Adv. Mater.* 12 (2000) 750–753. doi:10.1002/(SICI)1521-4095(200005)12:10<750::AID-ADMA750>3.0.CO;2-6.
- [36] H. Wan, F. Delale, L. Shen, Effect of CNT length and CNT-matrix interphase in carbon nanotube (CNT) reinforced composites, *Mech. Res. Commun.* 32 (2005) 481–489. doi:10.1016/j.mechrescom.2004.10.011.
- [37] S. Herasati, L.C. Zhang, H.H. Ruan, A new method for characterizing the interphase regions of carbon nanotube composites, *Int. J. Solids Struct.* 51 (2014) 1781–1791. doi:10.1016/j.ijsolstr.2014.01.019.

- [38] Z. Yuan, Z. Lu, M. Chen, Z. Yang, F. Xie, Interfacial properties of carboxylic acid functionalized CNT/polyethylene composites: A molecular dynamics simulation study, *Appl. Surf. Sci.* 351 (2015) 1043–1052. doi:10.1016/j.apsusc.2015.06.039.
- [39] A.B. Meddeb, T. Tighe, Z. Ounaies, O. Lopez-Pamies, Extreme enhancement of the nonlinear elastic response of elastomer nanoparticulate composites via interphases, *Compos. Part B Eng.* 156 (2019) 166–173. doi:10.1016/j.compositesb.2018.08.064.
- [40] N. Ning, T. Mi, G. Chu, L.Q. Zhang, L. Liu, M. Tian, H.T. Yu, Y.L. Lu, A quantitative approach to study the interface of carbon nanotubes/elastomer nanocomposites, *Eur. Polym. J.* 102 (2018) 10–18. doi:10.1016/j.eurpolymj.2018.03.007.
- [41] M.A.L. Monchado, L. Valentini, J. Biagotti, J.M. Kenny, Thermal and mechanical properties of single-walled carbon nanotubes–polypropylene composites prepared by melt processing, *Carbon N. Y.* 43 (2005) 1499–1505. doi:https://doi.org/10.1016/j.carbon.2005.01.031.
- [42] R. Andrews, D. Jacques, M. Minot, T. Rantell, Fabrication of Carbon Multiwall Nanotube / Polymer Composites by Shear Mixing, *Macromol. Mater. Eng.* 287 (2002) 395–403. doi:10.1002/1439-2054(20020601)287:6<395::AID-MAME395>3.0.CO;2-S.

APPENDIX A

The fictitious infinite medium in Mori-Tanaka type micromechanical models comprises of a homogenized medium that represents the entire composite in a continuum configuration. The only piece of information available about this C_{inf} beforehand is that it lies somewhere between the inclusion properties and the matrix properties (for a 2-phase system). Hence accurate use of such models requires an iterative approach in which the mechanical properties of the infinite medium are assigned assumed values and corrected in later iterations until the guesses assigned to the moduli are confirmed by the final composite moduli. For small inclusion volume fractions the moduli are expected to be much closer to those of the matrix than the inclusion. Using this information, in the isotropic case, we first assign the moduli of the matrix (polymer) to the infinite medium. Then after every calculation of the micromechanical model we check if the assumed Young's and shear moduli of the infinite medium are within 5% of the calculated composite moduli. If this condition is not satisfied the calculated moduli are assigned to the infinite medium and the calculations are restarted. This scheme resembles a fixed-point iteration algorithm. We found that the choice of initial guesses does not significantly affect the convergence. However, we plot how the accuracy requirement affects the convergence of the system in Figure 29. The horizontal axis represents the maximum tolerable error in the values of infinite medium Young's and shear moduli and the vertical axis shows the number of iterations necessary to converge using this tolerance.

This plot is obtained for the case of a CNT with 3.9 Å, using an interphase thickness of 5 Å and an exponential interphase moduli distribution with $a = 5$. The CNT aspect ratio was assumed to be 100.

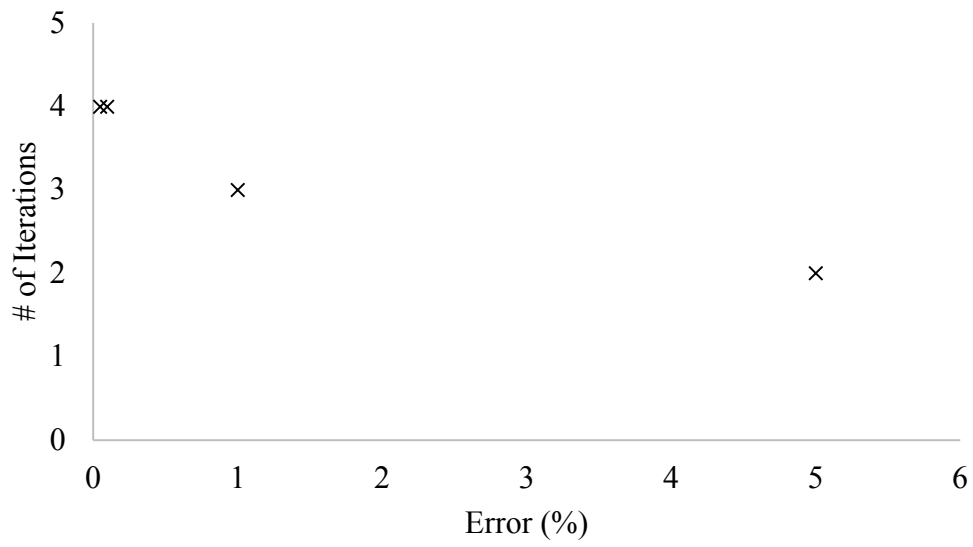


Figure 29. Number of iterations needed to converge given a maximum tolerance in infinite medium Young's and shear moduli.

APPENDIX B

Whereas this thesis is focused on the study of fiber-like inclusions, the model and methodologies developed can easily be adopted to analyze spherical and plate-like inclusions just as well. This can be used to study composites of graphene platelets, silica and fullerenes. To demonstrate this we study the effects of inclusion shape using a 3-phase micromechanical model in this appendix. The 3 phases consist of the inclusion, an interface and the matrix (bulk polymer). The interface is modelled in a position dependent manner where the moduli decay exponentially in the radially outward direction. The Young's modulus of the interface, E , in terms of Young's moduli of the inclusion and the bulk polymer, E_I and E_{BP} as

$$E(x) = \frac{E_{BP} - E_I}{e^{-\alpha} - 1} (e^{-\alpha x} - 1) + E_I \quad (32)$$

where a is the rate of exponential decay and it was set to 10 in this study.

We select three inclusions with cylindrical, spherical and plate-type shapes. The cylindrical inclusion has a radius of 5 Å and a length of 100 Å. The spherical inclusion has a radius of 5 Å and the plate type inclusion has a maximum thickness of 1 Å and a radius of 10 Å. The inclusion shapes are shown in Figure 30. Polyimide was selected to act as the matrix with a Young's modulus of 2.5 GPa and a Poisson's ratio of 0.34. The interface was assumed to have a thickness of 10 Å. The inclusion is assumed to have a Young's modulus of 1 TPa and a Poisson's ratio of 0.3 in all three cases. The orientations of the inclusion were then homogenized to simulate a composite with randomly distributed inclusion orientation. This results in an isotropic behavior of the nanocomposite.

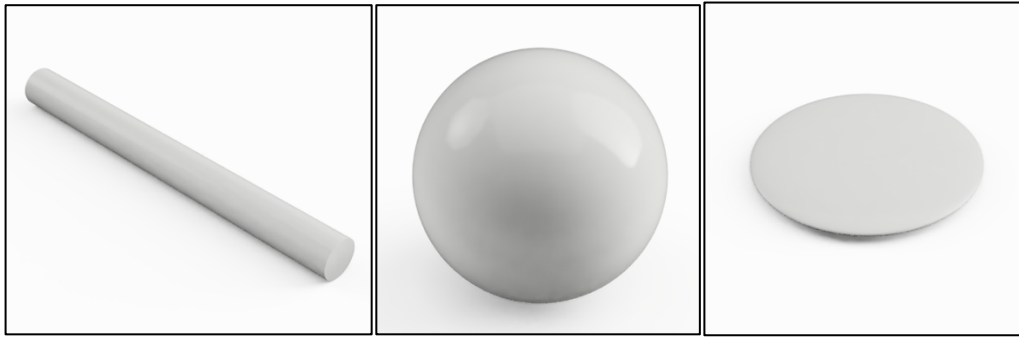


Figure 30. Cylindrical (left), spherical (center) and plate-like (right) inclusion shapes.

The cylindrical inclusion appears to have resulted in higher stiffening of the polymer as seen in Figure 31, followed by the spherical inclusion. The higher stiffening effect of the cylindrical inclusion is a result of its high aspect ratio. A high inclusion aspect ratio allows for greater adhesion with the polymer due to increased contact area.

While the plate like inclusion has a higher surface area to volume ratio, it is larger in volume than the spherical inclusion. For the same inclusion volume fraction decreasing the size of the inclusion is tantamount to increasing the number of inclusions which in turn results in higher interface volume fractions. Since the interface is stronger than the polymer, and hence helps reinforce it, increased interface volume fraction results in stiffer nanocomposites.

Next we investigate how the inclusion shape affects the performance. Figure 31 and Figure 32 depict variation in normalized composite stiffness with respect to cylindrical inclusion aspect ratio, defined as length of the cylinder divided by the diameter, and plate-like inclusion aspect ratio, defined as diameter of the plate divided by its width, respectively for an inclusion volume fraction of 1%. In both cases the composite stiffness rises until a point of saturation, where the contact surface area is large enough to efficiently transfer stress to the inclusion. The difference is, in the case of the cylindrical inclusion the curve saturates much earlier than plate-like inclusions. The curve of cylindrical inclusions appears to stabilize after an aspect ratio of 100, while that of plate-like inclusions does so an order of magnitude later, at around 1000 aspect

ratio. Furthermore, using a plate-like inclusion shape one can reach much higher stiffening ratios than using cylindrical inclusions.

In Figure 33 we study the effects of inclusion size on the composite moduli. The plots of Figure 33 show how nanocomposite stiffness varies by changing inclusion radii for an inclusion volume fraction of 1%. While all three inclusion shapes indicate exponential decay, they stabilize at different points. The top left plot shows how increasing inclusion size while keeping the shape the same affects the composite Young's modulus. The Young's modulus starts to level at around inclusion radius of 50 Å, while the other inclusion types start to stabilize at a radius of around 10 Å.

This loss in stiffness by increasing inclusion size is attributed to the decreased relative size of the interface. Larger structures result in decreased surface area to volume ratio. And since the volume of the interface depends on the contact area between the inclusion and the polymer, larger inclusions result in less interface and ergo a softer composite.

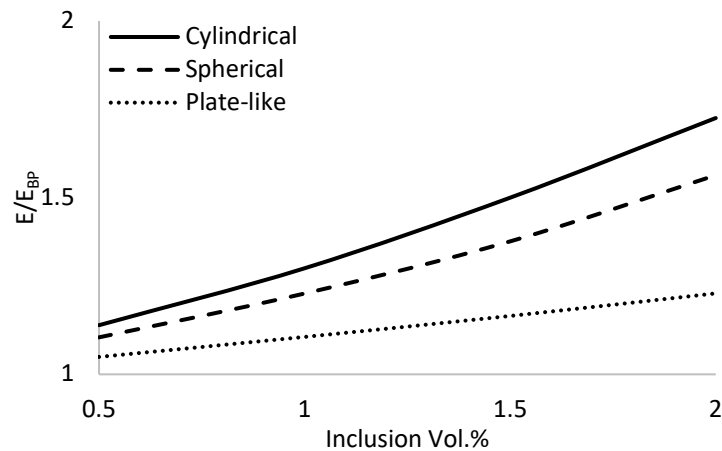


Figure 31. Variation of normalized composite Young's modulus, E/E_{BP} as a function of inclusion volume fraction for cylindrical, spherical and plate-like inclusions.

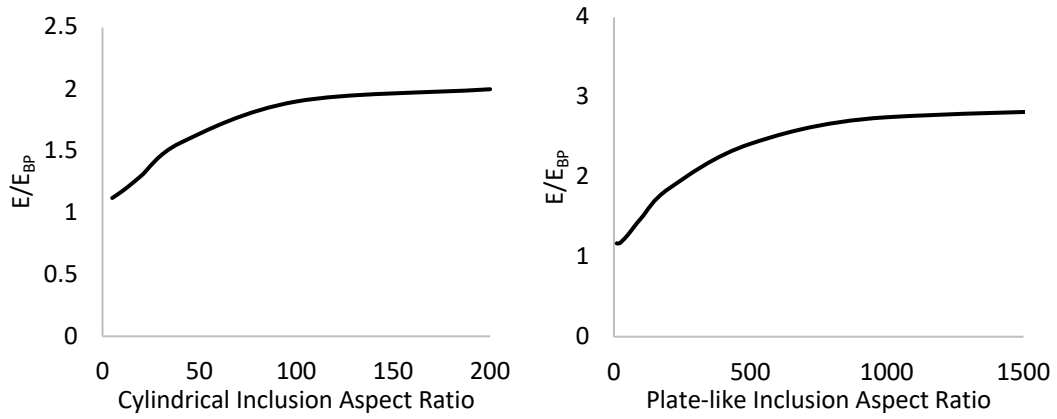


Figure 32. Variation of normalized composite Young's modulus as a function of cylindrical inclusion aspect ratio (left) and plate-like inclusion aspect ratio (right).

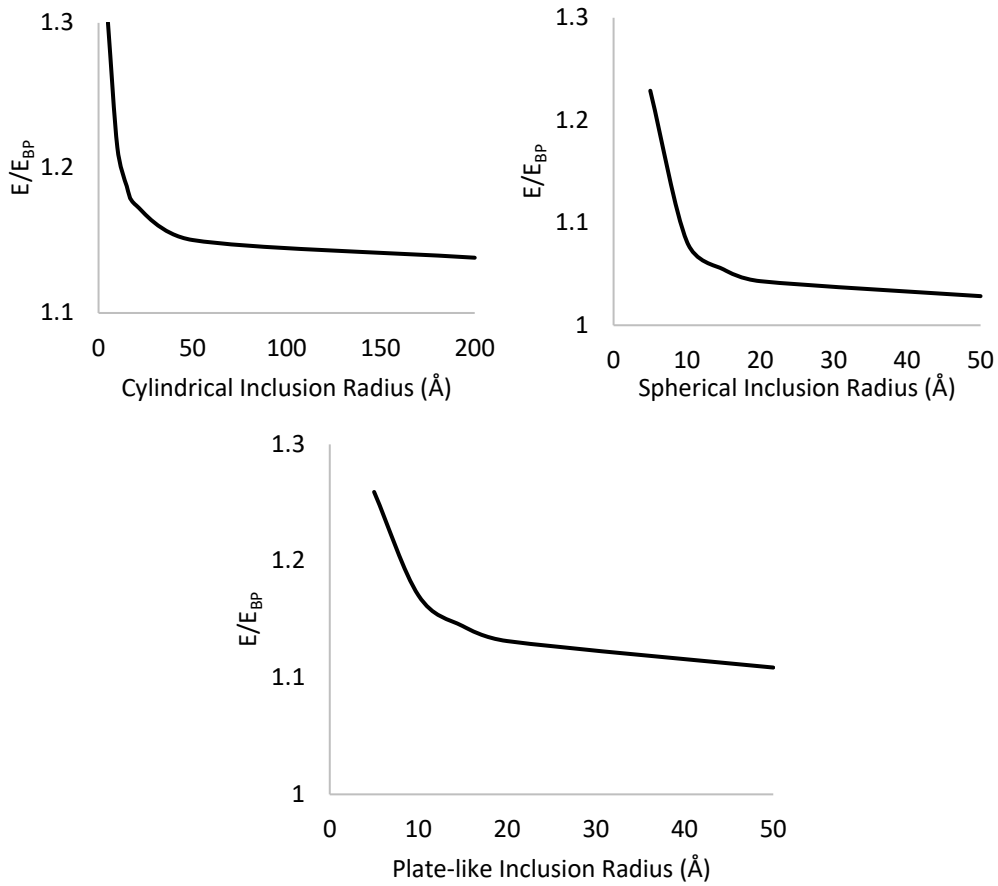


Figure 33. Variation of normalized composite stiffness with respect to cylindrical inclusion radius (top left), spherical inclusion radius (top right), and plate-like inclusion radius (bottom).

In conclusion, three different inclusion shapes were investigated for reinforcing polymeric materials in the nanometer scale; cylindrical, spherical and plate-like inclusions. The inclusions all have the same material properties which is roughly equal to those of carbon nanotubes. The interface was modelled in a graded manner using an exponentially decaying function. The cylindrical inclusion appears to perform better at low aspect ratios compared to the alternatives. This is because of the high surface area to volume fraction that such a geometry displays. However, one can increase the composite stiffness to much higher values using high aspect ratio plates.

APPENDIX C

Determination of the effective fiber elastic properties is a key task in modeling of carbon nanotube – polymer composites. In this study, we used the equivalence of displacements under a certain loading condition as a criterion for defining the effective fiber, such that the effective fiber should show similar displacements under given loading conditions as the actual carbon nanotube and interface combination. The loading conditions are summarized in **2.4.3 Effective Fiber (EF)**. Here we show in a detailed fashion how our effective fiber matches the carbon nanotube and interface combination (real model) and how the moduli of the effective fiber affect the displacements in those loading conditions. To study this effect, we multiplied the a given modulus by a factor α and observed how the displacements deviated from the real model. For example, $\alpha = 0.5$ means a given modulus of the effective fiber was halved, while everything else remained the same. Figure 34 shows this study for the case of axial compression. It is seen that no other modulus except for the axial Young's modulus (E_1) (shown with empty squares) affects the axial displacement in this loading condition in a significant fashion; thereby enabling the definitive determination of the axial Young's modulus. Next the radial displacement (normalized by the same displacement in the CNT – interface model under the same loading condition) in the radial loading case was plotted against α . This plot (Figure 35) indicates that two moduli, E_1 and E_2 affect the displacement. However, since E_1 was already fixed using Figure 34, the effect of this modulus can be eliminated; thus, allowing for the determination of E_2 . Following the same logic in Figure 36 allows for finding ν_{12} . This figure shows the normalized axial displacement under the same loading.

Last but not least, plotting hoop displacement under torsional loading shows that only shear modulus G_{12} affects this displacement component. Using a simple fitting procedure thus results in the determination of the value of G_{12} .

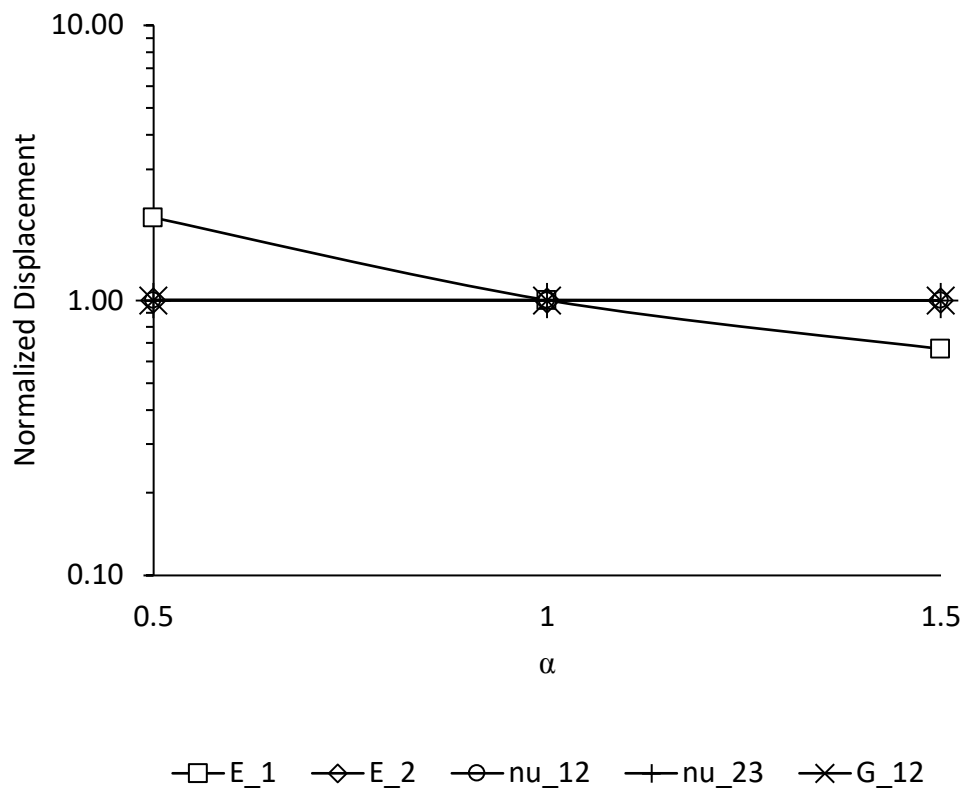


Figure 34. Variation of axial displacement in axial loading as a function of effective fiber moduli.

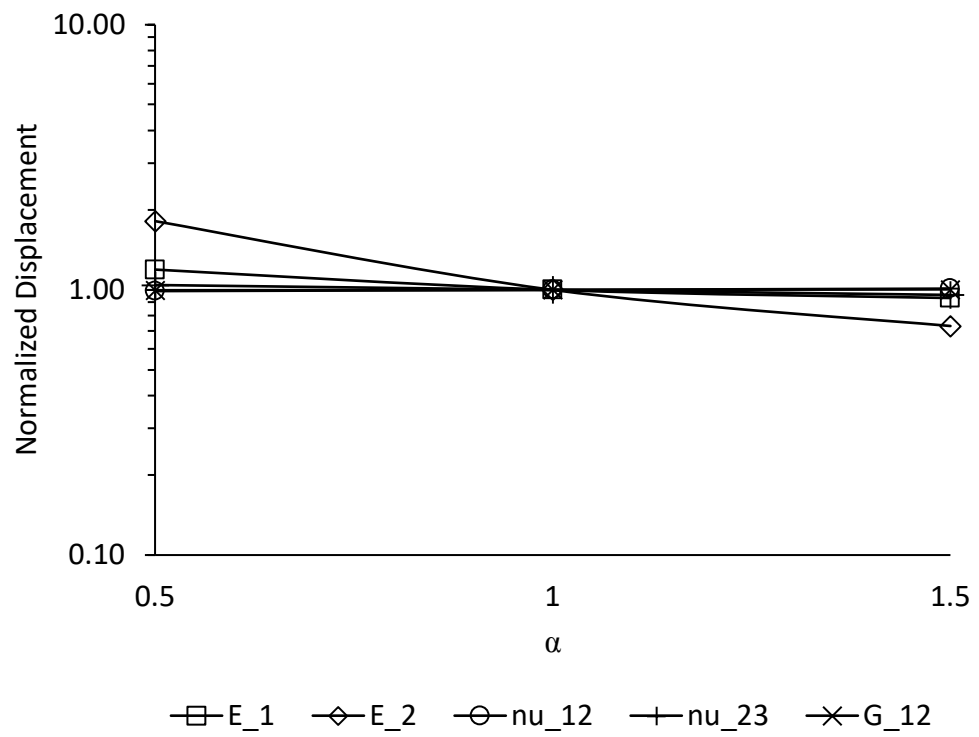


Figure 35. Variation of radial displacement in radial loading as a function of effective fiber moduli.

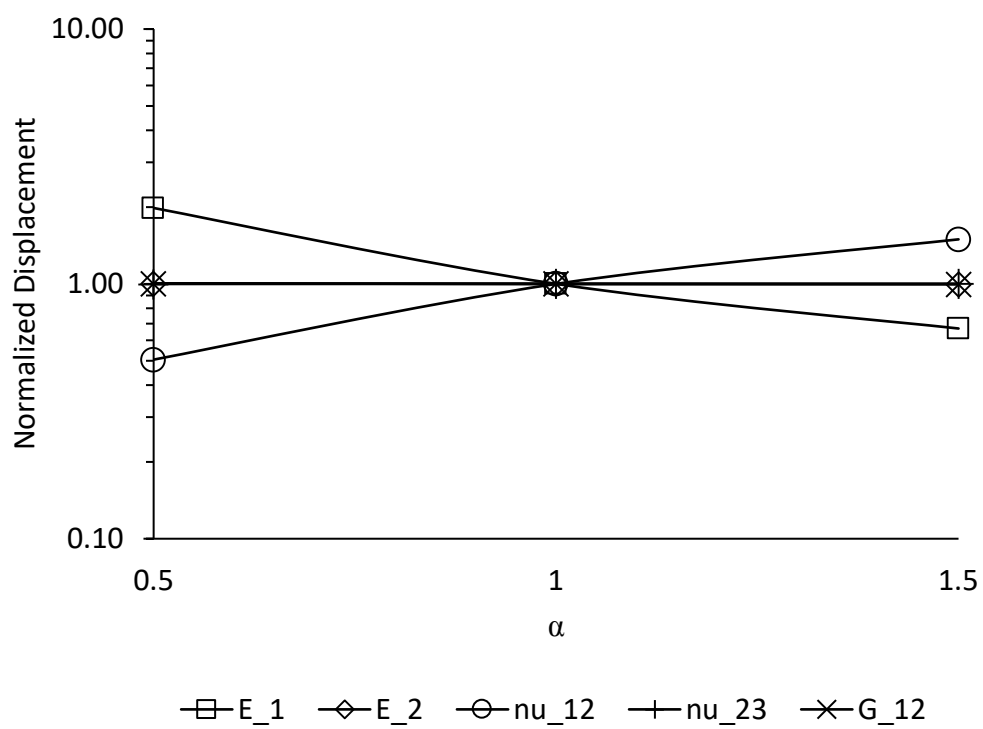


Figure 36. Variation of axial displacement in radial loading as a function of effective fiber moduli.

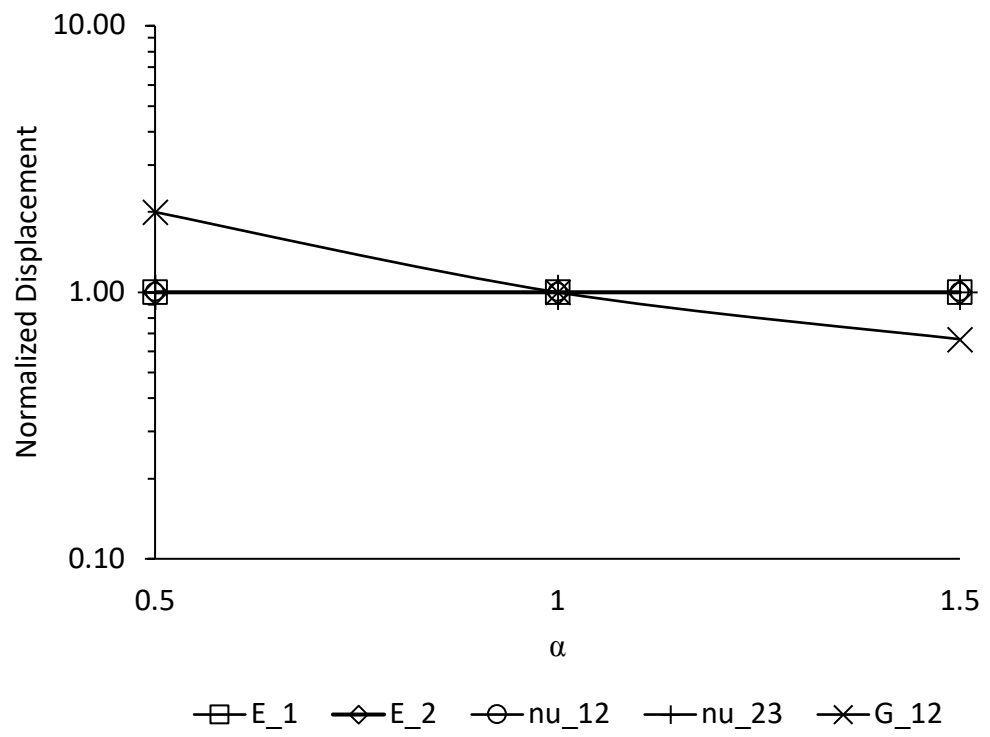


Figure 37. Variation of hoop displacement in torsional loading as a function of effective fiber moduli.